Layerwise models for supersonic flutter analysis of viscoelastic sandwich panels with curvilinear fibre composite skins

(Article begins on next page)

# Layerwise models for supersonic flutter analysis of viscoelastic sandwich panels with curvilinear fibre composite skins

J.A. Moreira [a],[*], F. Moleiro [a], A.L. Araújo [a], A. Pagani [b]

[a] IDMEC, Instituto Superior Tecnico, Universidade de Lisboa, Av. Rovisco Pais 1, Lisboa, 1049-001, Portugal
[b] MUL2, Department of Mechanical and Aerospace Engineering, Politecnico di Torino, Corso Duca degli Abruzzi 24, Torino, 10129, Italy

## ARTICLE INFO

## ABSTRACT

In this work, an assessment of layerwise finite element models for supersonic flutter analysis of soft core viscoelastic sandwich panels is presented, making use of various kinematic descriptions involving shear deformation theories and Lagrange $z$-expansions with thickness stretching, progressively refined to render numerically accurate and computationally efficient solutions. Numerical applications of sandwich panels include either viscoelastic or purely elastic core with skins of metal or laminated composite, using unidirectional or curvilinear fibres, considering thin and moderately thick panels, with core thickness ratios ranging from narrow to wide cores. A comprehensive assessment of the models predictive capabilities in free vibration analysis is carried out by comparison with three-dimensional exact solutions and numerical methods available in the literature. Even though it is concluded that layerwise first-order modelling, with no thickness stretching, ensures a fair compromise between numerical accuracy and computational efficiency in the aeroelastic flutter analysis of thin sandwich panels, layerwise high-order theories accounting for thickness stretching are rather necessary for the proper modelling of moderately thick sandwich panels, with either viscoelastic or purely elastic core.

## 1. Introduction

Noise and vibrations pose key design issues in most engineering fields within the transport industry, having a direct impact in competitive aspects involving comfort, safety and maintenance. More specifically, aerospace structures such as wings, control surfaces and fuselage skins are also prone to the occurrence of fluid induced vibrations and aeroelastic instabilities, which can lead to catastrophic failure or, at least, reduce the operating lifetime of critical components due to fatigue and crack growth. In light of the increasing interest in high-speed air-vehicles – such as space launchers, military fighters and operational unmanned aerial vehicles (UAVs) – having panel skins exposed to supersonic airflow, the complete understanding of panel flutter is of paramount importance, especially when dealing with multilayered structures involving non conventional materials, e.g. advanced composites with curvilinear fibres, metal–ceramic functionally graded mixtures or soft viscoelastic materials. Since the leading works on damped vibrations and damping treatments by DiTaranto et al. [1] and Mead and Markus [2], viscoelastic materials are frequently considered for reducing structural vibrations and noise radiation in lightweight sandwich structures. In fact, sandwich structures incorporating low density soft cores along with high stiff surface bonded skins (metal or composite) are a cornerstone in the current state-of-the-art regarding the design of aerospace structures, which is sustained by the exceptional compromise between strength and weight that can be achieved by combining these quite distinct materials. Nonetheless, the proper modelling of sandwich panels with high inhomogeneity of material properties through-thickness relies mostly on the application of Layerwise (LW) structural models [3,4],

---

capable of predicting accurate distributions of displacements and three-dimensional (3D) stresses at the layer level, including normal compressibility and transverse shear effects within the soft core, as shown by 3D elasticity solutions [5]. In addition, by considering variable stiffness composite (VSC) skins with curvilinear fibre paths, further modelling challenges are raised due to intricate in-plane stiffness distributions that may be exhibited, along with the characteristic bending–twisting coupling [6]. Still, it is worth mentioning that the curvilinear fibre composites technology has an emerging and highly promising potential for the design of aerospace structures, including improved buckling and first-ply failure responses [7], as well as enhanced aeroelastic stability of wings [8,9] and supersonic panels [10–12].

In view of the LW finite element (FE) modelling of viscoelastic sandwich panels with metal or composite skins, the combination of the Classical Plate Theory (CPT) for the skins and the First-order Shear Deformation Theory (FSDT) for the core [13–15] is one of the simpler kinematic descriptions that account for through-thickness continuous in-plane displacements, with zig-zag form, though neglecting thickness stretching. Despite being a computationally efficient LW approach, the assumption of no transverse shear in the skins (due to the CPT hypothesis) becomes less consistent as one considers moderately thick panels or materials more prone to exhibit significant shear deformations [16]. Hence, to account for shear deformation effects in the skins as well as in the viscoelastic core, LW FSDT models have been proposed [17,18], without increasing the computational cost as much as higher-order theories. Nonetheless, piecewise FSDT models still assume just constant through-thickness distributions of transverse shear stresses. Therefore, LW models making use of FSDT for the skins and Third-order Shear Deformation Theory (TSDT) for the core have also been introduced [19–22] aiming at a more realistic description of transverse shear deformations within the core and, consequently, ensuring a more accurate prediction of the energy dissipation (which is mainly induced by the shear deformation of the viscoelastic layer). Considering different kinematic refinements, the aforementioned LW models do not account for thickness stretching effects, which are greatly potentiated by the embedded soft core within the stiff face layers. Actually, both thickness stretching effects and transverse shear deformations play a fundamental role in the vibration response of certain modes in soft core sandwich panels, especially when not so thin panels are concerned [5], and, therefore, quasi-3D descriptions are necessary to accurately predict through-thickness mode shapes, natural frequencies, as well as modal loss factors in the case of viscoelastic core materials [23].

As regards to the application of LW models accounting for transverse normal strains, there are some noteworthy works in the literature [24–28] making use of the Carrera Unified Formulation (CUF) - thus allowing the accuracy assessment of various kinematic models, with any expansion-order, in a systematic and hierarchical manner. In particular, Ferreira et al. [24] and Liu et al. [25] considered a LW first-order model, with Lagrange *z*-expansion functions, for free vibration analysis of viscoelastic sandwich plates, using both the classical FE method and the differential quadrature hierarchical FE method. High-order LW models are indeed investigated by Filippi and Carrera [26] for vibration analysis of damped viscoelastic beams and circular rings, as well as by Filippi et al. [27] considering both LW and Zig-Zag descriptions for multilayered beams and plates embedding viscoelastic layers. Considering also high-order LW descriptions, Alaimo et al. [28] presented Navier type analytical solutions for free vibration and frequency response of viscoelastic sandwich plates. Moreover, resorting to the Sublaminate Generalized Unified Formulation (SGUF), D'Ottavio et al. [29] focused on the dynamic response of multi-core viscoelastic sandwich panels, highlighting that quasi-3D accuracy can be achieved through the assumption of sublaminates while resorting to fewer degrees of freedom (DOFs) than purely LW descriptions.

Even though material damping is indeed advantageous in reducing mechanical vibrations, it has a dual nature when dealing with non conservative aeroelastic systems [30]. Specifically, aerodynamic damping has always a stabilizing effect, whereas structural damping may have either a stabilizing or destabilizing contribution to the occurrence of panel flutter, as highlighted earlier by Oyibo [31] and further corroborated in more recent works [32,33]. Likewise, the dual nature of viscoelastic damping treatments in the aeroelastic stability of supersonic sandwich panels is also verified [34–38], though it is highlighted that flutter improvements are attainable through design optimization since the thickness ratios and material properties of the layers influence significantly the dynamic and aeroelastic characteristics. Moreover, non-linear flutter analysis of pure viscoelastic panels under supersonic flow and thermal loads [39,40] revealed that the viscoelastic damping has a direct impact on reducing the region of chaotic type motion in the post-flutter aero-thermal response, such that chaotic behaviour can be effectively regulated as multi- or single-periodic motion. However, for aeroelastic flutter analysis of supersonic sandwich panels with viscoelastic damping treatments, the adopted LW models tend to be the simpler ones, assuming the CPT for the skins and the FSDT for the core [34,35] or (full) piecewise FSDT displacements [36–38] and, therefore, no high-order shear terms nor thickness stretching are considered. In fact, even the Euler–Bernoulli Beam Theory is assumed in [39,40] to describe the heated viscoelastic panel in supersonic airflow. Despite the limited number of available literature on the assessment and comparison of high-order LW models for supersonic panel flutter analysis, it is worth remarking that Carrera and Zappino [41] and Zappino et al. [42] discussed variable-kinematic one-dimensional (1D) and bi-dimensional (2D) type CUF models, respectively, for flutter analysis of supersonic composite shells with non conventional boundary conditions. As a matter of fact, a prior work by Birman and Librescu [43] suggested that for certain boundary conditions, side-to-thickness ratios (associated to moderately thick plates) and composites with high anisotropy ratios, the accurate predictions of transverse shear stresses via high-order theories may be relevant for panel flutter analysis.

In this work, the role of refined kinematic models in supersonic flutter analysis of soft core viscoelastic sandwich panels is investigated, including high-order shear deformation terms and thickness stretching effects. The well-established First-order Piston Theory is adopted as aerodynamic model, as also considered in the aforementioned works on supersonic panel flutter. The main novelties of the present work consist of: (i) the application and assessment of variable-kinematic 2D type LW FE models, aimed at panel flutter analysis of soft core sandwich panels in supersonic airflow, with either viscoelastic or purely elastic core; (ii) the investigation of not only conventional sandwich configurations involving skins of metal and straight fibre composite, but also variable stiffness configurations with curvilinear fibre composite skins, while accounting for various levels of kinematic enrichment;
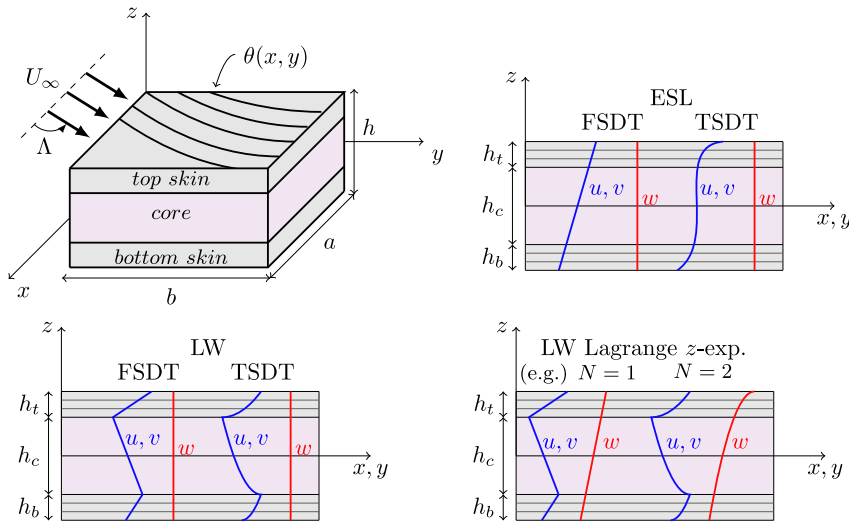
**Fig. 1.** Illustrative representation of a sandwich panel with (variable stiffness) laminated composite skins, taken as three discrete layers, under supersonic airflow: geometry and adopted structural theories.

and (iii) the aeroelastic response behaviour analysis of various sandwich configurations, discussing the effect of the core thickness ratio and viscoelastic loss factor.

To the best of the authors' knowledge, this is the first work providing an evaluation of LW models aimed at supersonic flutter analysis of viscoelastic sandwich panels, exploring both variable order shear deformation theories with no thickness stretching as well as quasi-3D models with full Lagrange $z$-expansions up to the third-order, while making progress on the combined application of curvilinear fibre composite laminates and soft core viscoelastic materials. The accuracy assessment of the models predictive capabilities is investigated considering both thin and moderately thick panels, either simply supported or clamped. Moreover, the effect of the core thickness ratio is also taken into account, including both narrow and wide cores. A comparison with available literature solutions is presented, considering 3D exact free vibration solutions for simply supported sandwich panels with purely elastic core by Moleiro et al. [5] as well as various FE solutions for free vibration analysis of viscoelastic sandwich panels [19,24,27]. Ultimately, the aeroelastic response behaviour of supersonic sandwich panels featuring skins of metal or laminated composite using unidirectional or curvilinear fibres is discussed, comparing purely elastic and viscoelastic core materials, with various loss factors, while highlighting proper modelling techniques suitable for aeroelastic control and design optimization applications.

## 2. Layerwise models

As intended in this work, multilayered structural models are developed considering a single core sandwich plate with top and bottom surface bonded elastic face layers (skins), taken as a set of three discrete layers – top ($t$), core ($c$) and bottom ($b$), as represented in the top left corner of Fig. 1 – under supersonic airflow on the upper surface with in-plane direction $\Lambda$. To be precise, each skin can be, in fact, another set of material/physical layers (sublaminate), corresponding most generally to variable stiffness composite layers with curvilinear fibre paths, i.e. a continuous fibre angle distribution $\theta(x, y)$.

Since the number of discrete layers is fixed, a multilayered skin is then treated as an Equivalent Single Layer (ESL) and, therefore, the computational efficiency of the LW models is not influenced by the number of actual material/physical layers within each skin. In fact, the use of a number of discrete layers different from the number of physical layers is indeed a common practice in the literature, including works regarding CUF framework [44,45] as well as the SGUF [29]. The ESL descriptions of the sandwich panels can actually be derived as particular cases of the LW descriptions involving just a unique discrete layer. As expected from 3D elasticity, ESL models are rather deficient in accounting for high inhomogeneity of material properties in general sandwich panels, not being capable of predicting the necessary zig-zag form in the through-thickness distributions of in-plane displacements, as illustrated in Fig. 1. To provide a brief, yet quite necessary comparison of LW and ESL descriptions, the FSDT and TSDT are both considered in each modelling framework, in addition to cubic Lagrange $z$-expansions with thickness stretching. In fact, the LW models make use of not only shear deformation theories but also further refined theories, exploring Lagrange $z$-expansions of all displacement components, with variable $N$-order, which allow transverse normal deformations to be captured due to the non constant through-thickness distribution of transverse displacements.

As a result, the models which account for transverse normal strains make use of 3D constitutive equations in complete agreement with linear elasticity, whereas shear deformation models resort to reduced plane stress constitutive equations (thus allowing the mitigation of thickness locking). In line with the SGUF nomenclature [29], the 3D stress–strain equations of the $p$-physical layer within the $k$-sublaminate (discrete layer) are written in the global reference system ($x, y, z$) as shown:

$$\boldsymbol{\sigma}^{kp} = \bar{\boldsymbol{C}}^{kp} \boldsymbol{\varepsilon}^{kp} \tag{1}$$

where the stresses $\boldsymbol{\sigma}^{kp}$ and the strains $\boldsymbol{\varepsilon}^{kp}$ are structured, according to Voigt notation, as follows:

$$\boldsymbol{\sigma}^{kp} = \left\{ \sigma_{xx}^{kp} \ \sigma_{yy}^{kp} \ \sigma_{zz}^{kp} \ \sigma_{yz}^{kp} \ \sigma_{xz}^{kp} \ \sigma_{xy}^{kp} \right\}^T \tag{2a}$$

$$\boldsymbol{\varepsilon}^{kp} = \left\{ \varepsilon_{xx}^{kp} \ \varepsilon_{yy}^{kp} \ \varepsilon_{zz}^{kp} \ \gamma_{yz}^{kp} \ \gamma_{xz}^{kp} \ \gamma_{xy}^{kp} \right\}^T \tag{2b}$$

Under the assumption of infinitesimal strains, the strain–displacement relations are given by:

$$\varepsilon_{xx}^{kp} = u_{,x}^{kp} \tag{3a}$$

$$\varepsilon_{yy}^{kp} = v_{,y}^{kp} \tag{3b}$$

$$\varepsilon_{zz}^{kp} = w_{,z}^{kp} \tag{3c}$$

$$\gamma_{yz}^{kp} = v_{,z}^{kp} + w_{,y}^{kp} \tag{3d}$$

$$\gamma_{xz}^{kp} = u_{,z}^{kp} + w_{,x}^{kp} \tag{3e}$$

$$\gamma_{xy}^{kp} = u_{,y}^{kp} + v_{,x}^{kp} \tag{3f}$$

where $u$, $v$ and $w$ are the displacement components in the $x$-, $y$- and $z$-axis, respectively, such that the displacement vector is $\boldsymbol{u} = \{u \ v \ w\}^T$.

The 3D elastic tensor is obtained by $\bar{\boldsymbol{C}}^{kp} = \boldsymbol{R}^T(\theta^{kp})\boldsymbol{C}^{kp}\boldsymbol{R}(\theta^{kp})$ due to the necessary in-plane rotation between the layer material reference system and the global one [46], where the components of the 3D elastic tensor in the material reference system $\boldsymbol{C}^{kp}$ of pointwise orthotropic materials, as well as the rotation matrix $\boldsymbol{R}(\theta^{kp})$ are given explicitly in [46]. Note that in the most general case of curvilinear fibre composite layers, the elastic coefficients in the global reference system are given as continuous functions, i.e. $\bar{\boldsymbol{C}}^{kp} = \bar{\boldsymbol{C}}^{kp}(x, y)$, in agreement with the prescribed fibre angle distribution $\theta^{kp}(x, y)$. More precisely, it is assumed in this work that each composite layer can have a linear fibre angle variation along the $x$-axis, expressed as follows:

$$\theta^{kp}(x) = T_0^{kp} + \frac{2(T_1^{kp} - T_0^{kp})}{a} \left| x - \frac{a}{2} \right| \tag{4}$$

where $<T_0^{kp}, T_1^{kp}>$ stands for the pair of control angles defined as $T_0^{kp} = \theta^{kp}(a/2)$ and $T_1^{kp} = \theta^{kp}(0) = \theta^{kp}(a)$ (where $a$ is the side along the $x$-axis).

Under the typical approach to develop models that neglect transverse normal strains ($\varepsilon_{zz}^{kp} = 0$), such as the shear deformation plate theories, it is further assumed the use of reduced plane stress constitutive equations by imposing $\sigma_{zz}^{kp} = 0$ in the 3D constitutive equations [46]. Hence, in the material reference system, the non zero components of the reduced elastic tensor $\boldsymbol{Q}^{kp}$ are derived from the ones of the 3D elastic tensor $\boldsymbol{C}^{kp}$ as follows:

$$Q_{ij}^{kp} = C_{ij}^{kp} - \frac{C_{i3}^{kp} C_{j3}^{kp}}{C_{33}^{kp}} \text{ for } i, j = 1, 2 \tag{5a}$$

$$Q_{ij}^{kp} = C_{ij}^{kp} \text{ for } i, j = 4, 5, 6 \tag{5b}$$

Following the necessary in-plane rotation [46], the reduced plane stress constitutive equations in the global reference system are then written as $\boldsymbol{\sigma}^{kp} = \bar{\boldsymbol{Q}}^{kp}\boldsymbol{\varepsilon}^{kp}$, where both $\sigma_{zz}^{kp}$ and $\varepsilon_{zz}^{kp}$ are not included.

Also noteworthy is that in the case of viscoelastic materials, the engineering constants are described using the complex modulus approach, i.e. the Young moduli, the shear moduli and the Poisson coefficients are characterized not only by a real part but also by an imaginary part, which is associated to the damping loss factor in that specific property. It is commonly assumed no damping factors in the Poisson coefficients, such that the engineering constants of a viscoelastic isotropic material can be reduced to the complex Young modulus $E = E^*(1 + i\eta)$ and to the real Poisson coefficient $v$. Accordingly, the resulting 3D elastic coefficients as well as the reduced elastic coefficients become complex. In the most general case, the real part of the Young modulus $E^*$ and the associated viscoelastic loss factor $\eta$ are both temperature- and frequency-dependent. Nonetheless, at this stage, such dependencies are not considered within the scope of the numerical applications herein. For ensuing works, it is also worth mentioning that since actual viscoelastic materials tend to present a highly nonlinear behaviour, advanced constitutive models are required to accurately capture the nonlinear stress–strain response [47–49]. However, when considering nonlinear viscoelastic constitutive models and/or temperature- and frequency-dependent material properties, an iterative scheme is required to solve the resulting nonlinear aero-visco-elastic equilibrium equations (thus leading to an increased computational time).

### 2.1. Shear deformation theories without thickness stretching

The FSDT and TSDT assume linear and cubic Taylor $z$-expansions for the in-plane displacements, respectively, along with a constant distribution of the transverse displacement [46]. Despite the well-known recommendations by Koiter [50], concerning the fact that a refinement of the shear terms would call for a refinement of the transverse normal behaviour regarding thickness stretching, it is worth mentioning that these models based on shear deformation theories devoid of thickness stretching typically involve a lower number of independent variables as compared to models which account for thickness stretching. Moreover, in view

of the LW modelling, the necessary continuity of the displacements at the interfaces between adjacent layers must be imposed *a priori*, as illustrated in Fig. 1. Imposing the interlaminar continuity of displacements, the LW TSDT displacement field of the three discrete layers is derived as shown:

$$u^c(x, y, z) = u_0^c(x, y) + z\theta_x^c(x, y) + z^2\varkappa_x^c(x, y) + z^3\lambda_x^c(x, y) \tag{6a}$$

$$v^c(x, y, z) = v_0^c(x, y) + z\theta_y^c(x, y) + z^2\varkappa_y^c(x, y) + z^3\lambda_y^c(x, y) \tag{6b}$$

$$u^t(x, y, z) = \alpha_1 u_0^c(x, y) + \alpha_2\theta_x^c(x, y) + \alpha_3\varkappa_x^c(x, y) + \alpha_4\lambda_x^c(x, y) + \left(\alpha_5 + (z - z_0^t)\right)\theta_x^t(x, y) + \left(\alpha_6 + (z - z_0^t)^2\right)\varkappa_x^t(x, y) +$$
$$\left(\alpha_7 + (z - z_0^t)^3\right)\lambda_x^t(x, y) \tag{6c}$$

$$v^t(x, y, z) = \alpha_1 v_0^c(x, y) + \alpha_2\theta_y^c(x, y) + \alpha_3\varkappa_y^c(x, y) + \alpha_4\lambda_y^c(x, y) + \left(\alpha_5 + (z - z_0^t)\right)\theta_y^t(x, y) + \left(\alpha_6 + (z - z_0^t)^2\right)\varkappa_y^t(x, y) +$$
$$\left(\alpha_7 + (z - z_0^t)^3\right)\lambda_y^t(x, y) \tag{6d}$$

$$u^b(x, y, z) = \beta_1 u_0^c(x, y) + \beta_2\theta_x^c(x, y) + \beta_3\varkappa_x^c(x, y) + \beta_4\lambda_x^c(x, y) + \left(\beta_5 + (z - z_0^b)\right)\theta_x^b(x, y) + \left(\beta_6 + (z - z_0^b)^2\right)\varkappa_x^b(x, y) +$$
$$\left(\beta_7 + (z - z_0^b)^3\right)\lambda_x^b(x, y) \tag{6e}$$

$$v^b(x, y, z) = \beta_1 v_0^c(x, y) + \beta_2\theta_y^c(x, y) + \beta_3\varkappa_y^c(x, y) + \beta_4\lambda_y^c(x, y) + \left(\beta_5 + (z - z_0^b)\right)\theta_y^b(x, y) + \left(\beta_6 + (z - z_0^b)^2\right)\varkappa_y^b(x, y) +$$
$$\left(\beta_7 + (z - z_0^b)^3\right)\lambda_y^b(x, y) \tag{6f}$$

$$w^c(x, y, z) = w^t(x, y, z) = w^b(x, y, z) = w_0(x, y) \tag{6g}$$

where the subscript 0 stands for the mid-plane location, $\theta_x^k$ and $\theta_y^k$ denote the rotations of the normals to the mid-plane about the $y$- and $x$-axes, respectively, $\varkappa_x^k$, $\varkappa_y^k$, $\lambda_x^k$ and $\lambda_y^k$ are the higher-order generalized displacements of each $k$-discrete layer. The mid-plane transverse coordinates are $z_0^t = (h_t + h_c)/2$ and $z_0^b = -(h_b + h_c)/2$. As derived from the interlaminar continuity, the variables $\alpha_n$ and $\beta_n$ are defined by:

$$\alpha_1 = 1, \ \alpha_2 = h_c/2, \ \alpha_3 = \alpha_2^2, \ \alpha_4 = \alpha_2^3, \ \alpha_5 = h_t/2, \ \alpha_6 = -\alpha_5^2, \ \alpha_7 = \alpha_5^3 \tag{7a}$$

$$\beta_1 = 1, \ \beta_2 = -h_c/2, \ \beta_3 = \beta_2^2, \ \beta4 = -\beta_2^3, \ \beta_5 = -h_b/2, \ \beta_6 = -\beta_5^2, \ \beta_7 = \beta_5^3 \tag{7b}$$

The displacement field presented in Eq. (6) includes implicitly other simpler kinematic models, which can be recovered when neglecting some specific terms. Firstly, the LW model making use of the FSDT for the top and bottom skins, while maintaining the TSDT for the core, is obtained by neglecting the high-order terms associated to $k = t$ and $b$ in Eqs. (6c) to (6f). Secondly, the piecewise FSDT model is recovered by neglecting all high-order terms in the expansions of the in-plane displacements, for the three discrete layers. Finally, the ESL FSDT and ESL TSDT models can also be defined by assuming that the core displacements ($k = c$) are valid for the whole thickness, with linear and cubic $z$-expansion terms, respectively. To be clear, the twenty one degrees of freedom (DOFs) associated to the LW TSDT are $\boldsymbol{d} = \{u_0^c\ v_0^c\ w_0^c\ \theta_x^c\ \theta_y^c\ \varkappa_x^c\ \varkappa_y^c\ \lambda_x^c\ \lambda_y^c\ \theta_x^t\ \theta_y^t\ \varkappa_x^t\ \varkappa_y^t\ \lambda_x^t\ \lambda_y^t\ \theta_x^b\ \theta_y^b\ \varkappa_x^b\ \varkappa_y^b\ \lambda_x^b\ \lambda_y^b\}^T$, whereas for the LW model with FSDT skins and TSDT core, only thirteen DOFs remain since the high-order generalized displacements of the skins are disregarded. For the LW FSDT, no high-order generalized displacement is included and therefore only nine DOFs remain. Ultimately, the DOFs associated to the (ESL) TSDT and FSDT are just the first nine and five variables, respectively, noting that the superscript layer index does not apply since the independent variables are now introduced for the whole sandwich.

In view of the constant through-thickness distribution of shear strains predicted by the FSDT, a shear correction factor $K_s$ is applied for the evaluation of transverse shear stresses [46]. On the contrary, the TSDT predicts a more realist distribution of transverse shear strains and, therefore, it does not require the introduction of a shear correction factor. In the present work, no shear corrections factor is introduced in the LW FSDT modelling - i.e., $K_s = 1$, as suggested by Birman and Bert [51], and followed by Moreira et al. [6,52] - while in the brief examples regarding the ESL FSDT, it is assumed the usual $K_s = 5/6$ [46].

### 2.2. Theories based on Lagrange z-expansions with thickness stretching

Refined kinematic descriptions with quasi-3D predictive capabilities include both discrete layer transverse shear effects and discrete layer transverse normal effects [46], which are attainable by assuming, for instance, that the through-thickness distributions of the displacements are described using $z$-expansions based on Lagrange functions (noting that these formulations are often overlooked in the literature regarding the aeroelastic flutter analysis of supersonic panels). The enrichment of the displacement distributions through each layer thickness is then obtained by adopting high-order Lagrange $z$-expansions, as necessary. Considering the same $N$-order Lagrange $z$-expansion for each displacement component within each discrete layer, the displacement vector of the $k$-layer $\boldsymbol{u}^k$ is straightforwardly written as follows:

$$\boldsymbol{u}^k(x, y, z) = \sum_{j=1}^{N+1} \varphi_j^k(z)\boldsymbol{u}_j^k(x, y) \tag{8}$$

where $\varphi_j^k$ is the Lagrange function in the $k$-layer thickness at the $j$-node and $\boldsymbol{u}_j^k = \{u_j^k\ v_j^k\ w_j^k\}^T$ is the associated displacement vector (i.e the nodal variables). The $N$-order Lagrange functions, through each layer thickness, in terms of the natural coordinate

$\zeta^k \in [-1, \ 1]$, are given by:

$$\varphi_j^k\left(\zeta^k\right) = \prod_{\substack{s=1 \\ s \neq j}}^{N+1} \frac{\zeta^k - \zeta^{k_s}}{\zeta^{k_j} - \zeta^{k_s}} \tag{9}$$

where $\zeta^k = 2(z - z_0^k)/h^k$, denoting $z_0^k$ and $h_k$ as the mid-plane $z$-coordinate and thickness of the $k$-discrete layer, respectively. In this work, it is considered, most specifically, LW Lagrange models with linear, quadratic or cubic expansions.

Since in Lagrange $z$-expansions the independent variables correspond to displacements at prescribed locations, equidistant within the layer thickness, the interlaminar continuity of displacements can be easily imposed by assembling the displacement variables at the interfaces between adjacent layers. Hence, for a LW description which makes use of $N$-order Lagrange thickness-expansions and $N_L$ discrete layers, the total number of independent DOFs is $(3N_L(N+1) - 3(N_L - 1))$, where $(N_L - 1)$ stands for the number of interfaces. For three discrete layers, as presented in Fig. 1, the through-thickness continuity of displacements implies that $\boldsymbol{u}_{N+1}^b = \boldsymbol{u}_1^c$ (bottom-core interface) and $\boldsymbol{u}_{N+1}^c = \boldsymbol{u}_1^t$ (core-top interface), resulting that the assembled DOFs of a generic $N$-order expansion are $\boldsymbol{d} = \{\boldsymbol{u}_1^{b^T} \ \boldsymbol{u}_2^{b^T} \ ... \ \boldsymbol{u}_{N+1}^{b^T} \ \boldsymbol{u}_2^{c^T} \ ... \ \boldsymbol{u}_{N+1}^{c^T} \ \boldsymbol{u}_2^{t^T} \ ... \ \boldsymbol{u}_{N+1}^{t^T}\}^T$.

It is worth noting that no shear correction factor is introduced when applying the linear LW Lagrange model. In addition, ESL descriptions making use of Lagrange $z$-expansions can also be obtained by assuming that the thickness functions apply to the whole thickness domain of the sandwich, thus dropping the superscript $k$ associated to the discrete layers. Actually, the only ESL model based on Lagrange $z$-expansions considered in some numerical applications involves cubic $z$-expansions to provide a comparison with the previously introduced ESL TSDT model devoid of thickness stretching.

## 3. Aero-visco-elastic equilibrium equations

The Principle of Hamilton is applied to derive the dynamic equilibrium of the viscoelastic sandwich panel exposed to supersonic airflow on its upper surface ($z = h/2$), assuming that the generated transverse aerodynamic pressure $\Delta p$ is described by the well-established First-order Piston Theory. Hence, considering the sandwich panel taken as $k$ discrete layers with in-plane surface $S = [0, a] \times [0, b]$ and thickness domain $h^k$, the variational formulation can be expressed in the following form:

$$\sum_k \int_S \int_{h^k} \delta\boldsymbol{\varepsilon}^{k^T}\boldsymbol{\sigma}^k + \rho^k \delta\boldsymbol{u}^{k^T}\ddot{\boldsymbol{u}}^k \ dz dS = \int_S \delta\boldsymbol{u}^{t^T}|_{\frac{h}{2}} \boldsymbol{e}_z \Delta p \ dS \tag{10}$$

where $\delta$ stands for the variational operator, the double-dot denotes the second time derivative, $\rho^k$ is the $k$-layer density and $\boldsymbol{e}_z = \{0 \ 0 \ 1\}^T$.

In light of the First-order Piston Theory [41,53,54], the transverse loading resulting from the pressure difference generated by the supersonic airflow with yaw angle $\Lambda$ comes out as shown:

$$\Delta p = -\lambda\left(w_{,x}\cos\Lambda + w_{,y}\sin\Lambda\right)|_{\frac{h}{2}} - \mu\dot{w}|_{\frac{h}{2}} \tag{11}$$

such that the dynamic pressure parameter $\lambda$ and aerodynamic damping $\mu$ are given by:

$$\lambda = \frac{\rho_\infty U_\infty^2}{(M_\infty^2 - 1)^{1/2}} \tag{12a}$$

$$\mu = \lambda \frac{(M_\infty^2 - 2)}{(M_\infty^2 - 1)} \frac{1}{U_\infty} \tag{12b}$$

where $\rho_\infty$, $U_\infty$ and $M_\infty$ denote the density, speed and Mach number of the free airflow. The contribution of the aerodynamic damping is actually neglected since its inclusion leads to slightly higher flutter bounds [32,33]. As a result, more conservative flutter analyses can be ensured, from a design standpoint, by imposing $\mu = 0$ in Eq. (11), as also followed in [10,12].

For conciseness, the FE formulation is presented making use of a general notation in matrix form, with the dimensions and components dependent on the adopted kinematic theory. Hence, for an arbitrary $k$-discrete layer, regardless of its $p$-physical layers, the 1D $z$-expansions and 2D FE approximations of $\boldsymbol{u}^k$ and $\boldsymbol{\varepsilon}^k$ are defined as follows:

$$\boldsymbol{u}^k = \boldsymbol{Z}^k \boldsymbol{N}^k \boldsymbol{d} \tag{13a}$$

$$\boldsymbol{\varepsilon}^k = \boldsymbol{S}^k \boldsymbol{B}^k \boldsymbol{d} \tag{13b}$$

where $\boldsymbol{Z}^k$ and $\boldsymbol{S}^k$ contain the $z$-expansion functions within the discrete layer thickness, while $\boldsymbol{N}^k$ and $\boldsymbol{B}^k$ establish the necessary FE approximations in-plane via 2D shape functions. To be precise, for ESL models involving a unique discrete layer, the dependency on the index $k$ does not apply. In LW models involving three discrete layers, one has $k = \{t, c, b\}$, as shown in Fig. 1. Additionally, the adopted 2D shape functions are quadratic Lagrange functions, corresponding to the standard nine-node quadrilateral element [46] (Q9), such that the element DOFs are structured as $\boldsymbol{d} = \{\boldsymbol{d}_1^T \ ... \ \boldsymbol{d}_9^T\}^T$, where $\boldsymbol{d}_i$ stands for the nodal DOFs. The C$^0$-interpolation in-plane, required by the adopted structural FE models, is then verified by the 2D Lagrange polynomials, thus ensuring the interelement continuity of primary variables (as in a conforming element).

Introducing the FE approximations given in Eq. (13), the constitutive relations in Eqs. (1) as well as the aerodynamic pressure distribution in Eq. (11) without aerodynamic damping effect, all together, into Eq. (10), gives rise to the element equilibrium

equations in line with the different kinematic models. In the end, the aeroelastic equilibrium equations of the element can then be written as follows:

$$\boldsymbol{M}\ddot{\boldsymbol{d}} + (\boldsymbol{K} + \lambda \boldsymbol{K}_a)\boldsymbol{d} = \boldsymbol{0} \tag{14}$$

where $\boldsymbol{M}$, $\boldsymbol{K}$ and $\lambda \boldsymbol{K}_a$ are the mass, stiffness and aerodynamic stiffness matrices, respectively.

As derived from the variational formulation and taking into account that, in the most general case, each $k$-discrete layer can represent a sublaminate with $N_p^k$ physical layers, the implied element matrices are given by:

$$\boldsymbol{M} = \sum_{k=t,c,b} \sum_{p=1}^{N_p^k} \int_{\Omega} \boldsymbol{N}^{k^T} \left( \int_{h^{kp}} \rho^{kp} \boldsymbol{Z}^{k^T} \boldsymbol{Z}^k dz \right) \boldsymbol{N}^k d\Omega \tag{15a}$$

$$\boldsymbol{K} = \sum_{k=t,c,b} \sum_{p=1}^{N_p^k} \int_{\Omega} \boldsymbol{B}^{k^T} \left( \int_{h^{kp}} \boldsymbol{S}^{k^T} \bar{\boldsymbol{C}}^{kp} \boldsymbol{S}^k dz \right) \boldsymbol{B}^k d\Omega \tag{15b}$$

$$\boldsymbol{K}_a = \int_{\Omega} \boldsymbol{N}^{t^T} \boldsymbol{Z}^{t^T} |_{\frac{h}{2}} \boldsymbol{e}_z \boldsymbol{e}_z^T \boldsymbol{Z}^t |_{\frac{h}{2}} \left( \boldsymbol{N}_{,x}^t \cos \Lambda + \boldsymbol{N}_{,y}^t \sin \Lambda \right) d\Omega \tag{15c}$$

where the tensor $\bar{\boldsymbol{C}}^{kp}$ must be replaced by $\bar{\boldsymbol{Q}}^{kp}$, in line with the reduced plane stress coefficients given in Eq. (5), when considering shear deformation theories devoid of thickness stretching.

The 1D integrals in each thickness domain $h^{kp}$ are obtained using exact integration, whereas the integration in the in-plane FE domain $\Omega$ is carried out numerically, using Gauss quadrature, with reduced integration for the shear terms of the stiffness matrix (Eq. (15b)) to avoid shear locking [46]. It is worth remarking that: (i) for curvilinear fibre composite layers, the fibre angle is evaluated at each integration point within an element to ensure the most accurate estimation of the elastic coefficients; (ii) for sandwich panels with a viscoelastic core described via complex modulus approach, the stiffness matrix (Eq. (15b)) has complex components, which are, most generally, both temperature- and frequency-dependent and (iii) even when neglecting both viscoelastic and aerodynamic damping terms in the aeroelastic equilibrium equations, the eigenvalue solutions end up complex, since the aerodynamic stiffness matrix is non-symmetric (as opposed to the remaining element matrices which are symmetric and positive semidefinite due to the variational FE formulation), thus leading to aeroelastic coupling in the vibration modes.

After the standard FE assemblage and imposition of boundary conditions, the global eigenvalue problem can be written as follows:

$$\left| \left( \boldsymbol{K} + \lambda \boldsymbol{K}_a \right) - s_n \boldsymbol{M} \right| = \boldsymbol{0} \tag{16}$$

where the complex eigenvalue of the $n$-mode is represented by $s_n = \omega_n^2(1 + ig_n)$, with $i = \sqrt{-1}$. Hence, for a given flow condition defined through the dynamic pressure parameter $\lambda$, the solution of the eigenvalue problem yields the natural frequencies ($\omega_n$) and modal loss factors ($g_n$). Moreover, the particular case of free vibration in vacuum is obtained by setting $\lambda = 0$ in Eq. (16).

In short, as the dynamic pressure parameter $\lambda$ increases, flutter occurs as soon as the modal loss factor of one mode becomes negative, such that the system is dynamically unstable above the critical flutter dynamic pressure parameter $\lambda_F$. Actually, in the absence of dissipative terms (e.g., viscoelastic and aerodynamic damping), all modes show zero damping prior to the flutter bound and mode coalescence as flutter occurs explicitly [12], i.e. the eigenvalues of the modes involved in flutter emerge as complex conjugated pairs and the associated natural frequencies coalesce to the same frequency value, also known as flutter frequency $\omega_F$. However, in the presence of viscoelastic damping, single mode flutter can occur instead and, therefore, there is no coalescence of natural frequencies to a given flutter frequency, as carefully highlighted in the numerical applications. Furthermore, in general most viscoelastic materials show a temperature- and frequency-dependent elastic behaviour, which is directly translated to the stiffness matrix given in Eq. (15b). As a result, for a given dynamic pressure parameter, the solution of the eigenvalue problem stated in Eq. (16) requires an iterative solution procedure (see Araújo et al. [19] and D'Ottavio et al. [29] for further details). As regards to flutter analysis, which *per se* requires several iterations on $\lambda$ until $\lambda_F$ can be found for a specific tolerance, these material dependencies will further increase the computational effort/time to obtain accurate aeroelastic solutions. Hence, in view of the scope of the present work at this stage, these dependencies are not considered in the numerical applications. Nonetheless, by selecting the most computationally efficient yet fairly accurate model among the proposed kinematic theories, this work may point out the most suitable structural modelling approach for further aeroelastic analysis of general viscoelastic sandwich panels, incorporating materials with temperature- and/or frequency-dependent material properties, while ensuring that the multiple eigenvalues extractions are carried out as fast as possible, as also desired for design optimization purposes.

## 4. Numerical applications

The numerical applications are organized in two main parts: (i) Section 4.1 is focused on the free vibration and panel flutter analysis of simply supported sandwich panels with purely elastic soft core and unidirectional composite skins and provides a first assessment of the models predictive capabilities by comparison with 3D exact free vibration solutions as well as 3D Abaqus elements; and (ii) Section 4.2 is concerned with the aeroelastic flutter analysis of (soft core) viscoelastic sandwich panels with skins of metal or laminated composite using unidirectional or curvilinear fibres, considering both simply supported and clamped boundary conditions. In addition to thin panels, which are of primary interest for most aerospace applications, the response of moderately thick panels is also investigated to trigger more complicated effects that may occur, relying mostly on enriched kinematic models to be properly

captured. Besides, composite sandwich panels can be thicker without compromising structural weight as much as conventional metal ones.

Section 4.2 represents indeed the kernel of the present work and, therefore, it encompasses three steps: (i) a detailed convergence analysis, including both free vibration and panel flutter responses; (ii) a comparison with available free vibration solutions in the literature [20,24,27] (namely, a thin sandwich with metal skins and narrow viscoelastic core); and (iii) a comprehensive assessment of the models predictive capabilities in supersonic flutter analysis, considering both thin and moderately thick sandwich panels, with core thickness ratios ranging from narrow to wide cores.

All flutter solutions are presented for airflow along the x-axis (i.e., yaw angle $\Lambda = 0°$, Fig. 1) and the flutter dynamic pressure parameters $\lambda_F$ are given in the following nondimensionalized form:

$$\tilde{\lambda}_F = \frac{\lambda_F a^3}{h^3 G_0} \tag{17}$$

where $G_0$ stands for the reference shear modulus, which is selected for each test case, in accordance with the material properties of the face layers. The nondimensionalized flutter dynamic pressure parameters $\tilde{\lambda}_F$ are estimated using an iterative process, where the natural frequencies and modal loss factors of the modes of interest for flutter analysis are evaluated according to the eigenvalue problem defined in Eq. (16), considering increasing values of dynamic pressure parameter $\tilde{\lambda}$ until one mode has negative modal loss factor. The solution is then refined for the desired precision in terms of flutter bound. Hence, the iterative process converges when the difference between two successive values of dynamic pressure parameter – the first associated with a dynamically stable system and the second concerning an unstable system with at least one mode having a negative modal loss factor – is lower than a given convergence tolerance $\Delta\tilde{\lambda}$, where $\Delta\tilde{\lambda} = 0.001$ if $\tilde{\lambda}_F < 100$, or $\Delta\tilde{\lambda} = 0.01$ if $\tilde{\lambda}_F \geq 100$. In other words, this means that for a value of nondimensionalized pressure parameter $\tilde{\lambda} = \tilde{\lambda}_F - \Delta\tilde{\lambda}$, all modes are dynamically stable ($g_n \geq 0$), whereas for $\tilde{\lambda} = \tilde{\lambda}_F$, i.e. at the flutter bound, the system becomes dynamically unstable.

To be clear, the simply supported boundary conditions imposed, at the layer level, are as follows:

$$u^k = w^k = 0 \text{ at } y = 0, b \tag{18a}$$

$$v^k = w^k = 0 \text{ at } x = 0, a \tag{18b}$$

whereas for clamped plates, all displacements components are constrained in all four edges.

As regards to the adopted nomenclature for the models, the LW prefix is explicitly indicated prior to the kinematic theory, as in LW FSDT, LW TSDT or LW LagN, and therefore, any ESL prefix is omitted, as unnecessary. For brevity, the LW model involving FSDT for the skins and TSDT for the core is denoted by LW F/T/F, thus resembling the stacking sequence of the three discrete layers in terms of shear deformation theories, i.e. FSDT/TSDT/FSDT.

### 4.1. Sandwich panels with purely elastic core

A first assessment of the models predictive capabilities is carried out by comparison with 3D exact free vibration solutions by Moleiro et al. [5] and 3D elements available in the commercial software Abaqus, considering simply supported sandwich panels with purely elastic soft core along with unidirectional fibre reinforced composite layers of 0°. In line with earlier 3D exact solutions by Pagano [55], as also followed by Moleiro et al. [5], the test cases consist of square panels with side-to-thickness ratio $a/h = 100$ and 10, addressing the case of thin and moderately thick plates, respectively. Moreover, the core thickness is $8h/10$, thus the thickness of each composite skin is $h/10$. In particular, it is considered panels with $a = b = 1.2$ m. Assuming $E_0 = 7$ GPa and $\rho_0 = 1600$ kg/m³, the transversely isotropic soft core material properties are: $E_1 = E_2 = 0.04E_0$, $E_3 = 0.5E_0$, $G_{12} = 0.016E_0$, $= G_{13} = G_{23} = 0.06E_0$, $v_{12} = 0.25$, $v_{13} = v_{23} = 0.02$ and $\rho = 0.1\rho_0$; whereas the orthotropic composite layers material properties are: $E_1 = 25E_0$, $E_2 = E_3 = E_0$, $G_{12} = G_{13} = 0.5E_0$, $G_{23} = 0.2E_0$, $v_{12} = v_{13} = v_{23} = 0.25$ and $\rho = \rho_0$. Since the 3D exact free vibration solutions reported by Moleiro et al. [5] do not include explicitly the case of thin panels, further benchmark solutions are obtained making use of 3D Abaqus native elements, namely quadratic solid elements (C3D20R), applying a mesh of $14 \times 14$ elements in-plane, along with seven elements in the thickness direction: two per composite layer plus three for the core. The present 2D FE solutions are obtained using a mesh of $14 \times 14$ Q9 elements, which ensures converged solutions. At this point, a convergence analysis is omitted, for brevity, but it is presented in the following subsection, considering the analysis of viscoelastic sandwich panels.

Table 1 presents the free vibration results, alongside 3D exact solutions and 3D Abaqus predictions, as well as the brand new aeroelastic panel flutter solutions predicted by the present models. The free vibration solutions include the first twelve nondimensionalized natural frequencies in vacuum $\tilde{\omega}_{mn} = \omega_{mn}\sqrt{\rho_0/E_0}(a^2/h)$ (where m and n stand for the number of half-waves in the x- and y-axis, respectively). The aeroelastic solutions consist of flutter dynamic pressure parameters $\tilde{\lambda}_F$, nondimensionalized according to Eq. (17) with $G_0 = G_{12}^{skin} = 0.5E_0$, and nondimensionalized flutter frequencies $\tilde{\omega}_F = \omega_F\sqrt{\rho_0/E_0}(a^2/h)$.

Among the first twelve natural frequencies presented in Table 1, there are solely bending modes in the case of thin panels ($a/h = 100$), whereas for moderately thick panels ($a/h = 10$), two pairs of purely extensional modes without transverse displacement emerge amid the bending modes, as indicated by either $m = 0$ or $n = 0$. Additionally, the eighth natural frequency of the moderately thick panel corresponds, in fact, to the second thickness mode associated to the in-plane mode $(1, 1)$, as shown in detail by the 3D exact solutions [5]. Regarding the free vibration analysis, the numerical results given in Table 1 lead to the following conclusions:

**Table 1**

First twelve natural frequencies $\tilde{\omega}_{mn}$, flutter dynamic pressure parameters $\tilde{\lambda}_F$ and flutter frequencies $\tilde{\omega}_F$ of simply supported sandwich panels with purely elastic core (nondimensionalized results).

| $a/h$ | Model | $\tilde{\omega}_{11}$ | $\tilde{\omega}_{12}$ | $\tilde{\omega}_{13}$ | $\tilde{\omega}_{14}$ | $\tilde{\omega}_{21}$ | $\tilde{\omega}_{22}$ | $\tilde{\omega}_{23}$ | $\tilde{\omega}_{15}$ | $\tilde{\omega}_{24}$ | $\tilde{\omega}_{25}$ | $\tilde{\omega}_{16}$ | $\tilde{\omega}_{31}$ | $\tilde{\lambda}_F$ | $\tilde{\omega}_F$ [b] |
|---|---|---|---|---|---|---|---|---|---|---|---|---|---|---|---|
| 100 | 3D Abaqus | 20.002 | 26.996 | 43.141 | 68.296 | 74.014 | 78.140 | 87.928 | 101.697 | 105.896 | 133.227 | 142.994 | 159.118 | – | – |
| | FSDT | 20.083 | 27.079 | 43.235 | 68.433 | 75.210 | 79.364 | 89.169 | 101.930 | 107.145 | 134.516 | 143.398 | 164.639 | 703.45 | 62.575 |
| | TSDT | 20.017 | 27.012 | 43.160 | 68.324 | 74.238 | 78.370 | 88.163 | 101.747 | 106.138 | 133.482 | 143.082 | 160.131 | 691.99 | 62.220 |
| | Lag3 | 20.050 | 27.143 | 43.472 | 68.880 | 74.299 | 78.500 | 88.445 | 102.611 | 106.664 | 134.337 | 144.323 | 160.243 | 693.10 | 62.274 |
| | LW FSDT | 20.002 | 26.996 | 43.142 | 68.296 | 74.018 | 78.145 | 87.936 | 101.695 | 105.910 | 133.244 | 142.988 | 159.137 | 689.40 | 62.140 |
| | LW F/T/F | 20.002 | 26.996 | 43.142 | 68.295 | 74.018 | 78.145 | 87.936 | 101.695 | 105.909 | 133.244 | 142.988 | 159.137 | 689.40 | 62.140 |
| | LW TSDT | 20.002 | 26.996 | 43.141 | 68.293 | 74.012 | 78.139 | 87.930 | 101.689 | 105.902 | 133.234 | 142.977 | 159.112 | 689.33 | 62.138 |
| | LW Lag1 | 20.004 | 27.001 | 43.154 | 68.320 | 74.021 | 78.151 | 87.949 | 101.736 | 105.935 | 133.288 | 143.058 | 159.146 | 689.47 | 62.141 |
| | LW Lag2 | 20.002 | 26.996 | 43.143 | 68.299 | 74.014 | 78.142 | 87.935 | 101.703 | 105.912 | 133.252 | 143.008 | 159.119 | 689.38 | 62.138 |
| | LW Lag3 | 20.002 | 26.996 | 43.143 | 68.299 | 74.014 | 78.142 | 87.935 | 101.703 | 105.911 | 133.252 | 143.008 | 159.119 | 689.38 | 62.138 |

| $a/h$ | Model | $\tilde{\omega}_{11}$ | $\tilde{\omega}_{12}$ | $\tilde{\omega}_{10}$ | $\tilde{\omega}_{01}$ | $\tilde{\omega}_{21}$ | $\tilde{\omega}_{13}$ | $\tilde{\omega}_{22}$ | $\tilde{\omega}_{11-2}$ [a] | $\tilde{\omega}_{23}$ | $\tilde{\omega}_{20}$ | $\tilde{\omega}_{02}$ | $\tilde{\omega}_{14}$ | $\tilde{\lambda}_F$ | $\tilde{\omega}_F$ [c] |
|---|---|---|---|---|---|---|---|---|---|---|---|---|---|---|---|
| 10 | 3D Exact [5] | 12.643 | 18.690 | 19.936 | 19.936 | 28.182 | 29.826 | 31.727 | 34.666 | 39.560 | 39.848 | 39.850 | 43.499 | – | – |
| | 3D Abaqus | 12.643 | 18.690 | 19.936 | 19.936 | 28.183 | 29.832 | 31.727 | 34.666 | 39.563 | 39.849 | 39.851 | 43.530 | – | – |
| | FSDT | 14.998 | 19.940 | 19.940 | 20.797 | 32.081 | 34.687 | 36.981 | 39.881 | 39.881 | 39.975 | 46.492 | 47.097 | 292.26 | 48.056 |
| | TSDT | 12.992 | 19.002 | 19.938 | 19.939 | 29.346 | 30.212 | 32.797 | 34.679 | 39.867 | 39.875 | 40.571 | 44.113 | 204.01 | 42.372 |
| | Lag3 | 13.025 | 19.133 | 19.938 | 19.939 | 29.383 | 30.488 | 32.923 | 34.761 | 39.867 | 39.875 | 40.841 | 44.555 | 226.69 | 44.761 |
| | LW FSDT | 12.646 | 18.683 | 19.940 | 19.940 | 28.214 | 29.814 | 31.740 | 34.686 | 39.565 | 39.880 | 39.881 | 43.515 | 189.56 | 41.074 |
| | LW F/T/F | 12.646 | 18.683 | 19.936 | 19.936 | 28.214 | 29.813 | 31.740 | 34.668 | 39.564 | 39.850 | 39.851 | 43.512 | 189.56 | 41.074 |
| | LW TSDT | 12.637 | 18.669 | 19.936 | 19.936 | 28.184 | 29.783 | 31.709 | 34.668 | 39.521 | 39.850 | 39.851 | 43.455 | 189.33 | 41.064 |
| | LW Lag1 | 12.653 | 18.708 | 19.940 | 19.940 | 28.228 | 29.877 | 31.778 | 34.685 | 39.644 | 39.880 | 39.881 | 43.636 | 207.21 | 42.996 |
| | LW Lag2 | 12.643 | 18.691 | 19.936 | 19.936 | 28.185 | 29.834 | 31.729 | 34.666 | 39.566 | 39.850 | 39.851 | 43.534 | 209.88 | 43.398 |
| | LW Lag3 | 12.643 | 18.690 | 19.936 | 19.936 | 28.183 | 29.833 | 31.727 | 34.666 | 39.564 | 39.850 | 39.851 | 43.530 | 209.99 | 43.416 |

[a] (second) thickness mode.

[b] Flutter due to the second and third modes.

[c] Flutter due to the seventh and eighth modes.

- ESL descriptions seem to be rather deficient in accuracy – regardless of making use of high-order theories, with or without thickness stretching – providing overestimated natural frequencies, even when thin sandwich panels are considered. Hence, highlighting the need for LW modelling in multilayered structures with high inhomogeneity of material properties through-thickness.

- The proposed LW models predict the first twelve natural frequencies of thin sandwich panels in excellent agreement with the 3D Abaqus elements. Therefore, the LW FSDT model ensures the better compromise between numerical accuracy and computational efficiency when dealing with thin panels.

- Even though the natural frequencies predicted by LW Lag1 model are fairly accurate, it is interesting to remark that they are overestimated in comparison to the remaining set of LW models due to thickness locking, which can be effectively mitigated by assuming either plane stress constitutive equations (as in the shear deformation models) or high-order $z$-expansions in the transverse displacements (as in the LW Lag$N$ models, with $N \geq 2$). Thickness locking, also known as Poisson locking, arises due to the use of simplified kinematic assumptions in the analysis of plates/shells and is significantly dependent on the inherent coupling between out-of-plane and in-plane normal strains in the 3D constitutive law (see [56,57] for further details).

- As far as moderately thick panels are considered, the LW models based on Lagrange $z$-expansions (hereafter simply called LW Lagrange models) are capable of rendering highly accurate free vibration predictions, in agreement with 3D exact solutions and 3D Abaqus elements, including bending modes, purely extensional modes as well as high-order thickness modes. In particular, there is no significant advantage of applying cubic Lagrange $z$-expansions over quadratic.

To provide a further understanding on the aeroelastic flutter response behaviour of sandwich panels with purely elastic soft core, Fig. 2 represents the evolution of the first ten natural frequencies and damping factors with the increase of the dynamic pressure parameter (nondimensionalized results), considering both side-to-thickness ratios. Furthermore, Fig. 2 includes not only the results obtained by the most refined model (LW Lag3), in subtle solid lines, but also the LW F/T/F solutions, in dashed lines.

As perceived from the frequency and damping diagrams, mode coalescence as flutter occurs, involving the second and third modes for $a/h = 100$, as well as the seventh and eighth modes for $a/h = 10$. In fact, as the natural frequencies coalesce, the eigenvalues associated to these modes emerge as complex conjugated pairs, yielding a negative damping factor for the dynamic pressure parameters above the critical flutter bound. Since the aerodynamic and viscoelastic damping are both neglected, all modes show a null damping factor prior to the flutter bound. For thin panels with $a/h = 100$, the aforementioned two models predict the evolution of the natural frequencies and damping factors in excellent agreement with each other, but for moderately thick panels with $a/h = 10$, some discrepancies between the models become perceptible for high values of dynamic pressure parameter, around the flutter bound. To be precise, the LW F/T/F model predicts a 10% lower flutter dynamic pressure parameter than the LW Lag3 model, which is quite noticeable in the sign change of damping factors shown in Fig. 2.

Considering the flutter analyses, the numerical results provided in Table 1 also demonstrate that ESL models seem to be rather deficient in accuracy for the modelling of soft core sandwich panels, overpredicting the flutter dynamic pressure parameters even
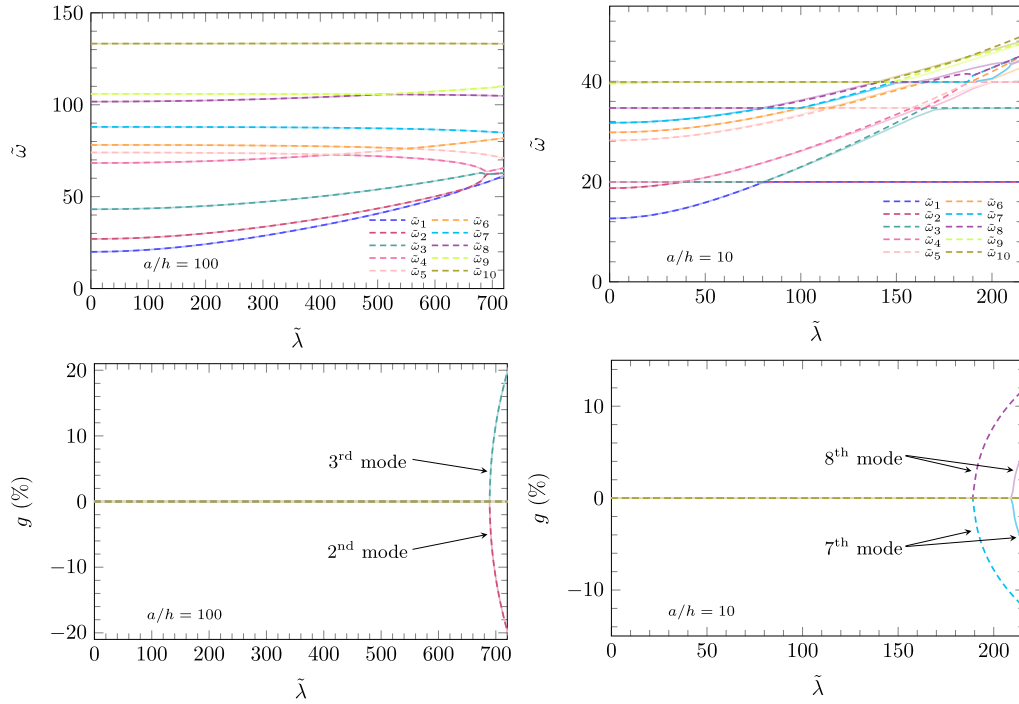
**Fig. 2.** Variation of the first ten nondimensionalized natural frequencies $\tilde{\omega}_n$ and damping factors $g_n$ with the nondimensionalized pressure parameter $\tilde{\lambda}$ of simply supported sandwich panels with purely elastic core: LW Lag3 (solid lines) and LW F/T/F (dashed lines) models.

when dealing with thin panels. The only exception is indeed the TSDT models in the case of panels with $a/h = 10$. In terms of LW modelling, there is no advantage of using TSDT for the core over FSDT in the present flutter analyses. As a result, the piecewise FSDT model ensures the fairest trade-off between numerical accuracy and computational efficiency for flutter analysis of supersonic sandwich panels, as also concluded for free vibration analysis. Moreover, the comparison between the ESL TSDT and the ESL Lag3 models reveals that the inclusion of transverse normal deformations and the use of 3D constitutive equations leads to higher flutter bounds and higher flutter frequencies. This is also perceived from the comparison between the LW TSDT and the LW Lag3 models. In fact, among the proposed models, the LW TSDT predicts the lowest flutter dynamic pressure parameters for both side-to-thickness ratios. Nonetheless, it is pointed out that the inclusion of thickness stretching influences significantly the aeroelastic response of the moderately thick sandwich panel, as opposed to the case of the thin panel. More precisely, for the thin panel, a higher expansion order $N$ leads to lower flutter dynamic pressure parameters, but for the moderately thick panel, an opposite trend is perceived. In particular, for thin plates with $a/h = 100$, there is no difference in the predicted flutter bound when using $N = 3$ or $N = 2$.

All in all, this initial benchmark demonstrates the key role of LW descriptions to properly capture the aeroelastic flutter response behaviour of supersonic soft core sandwich panels as well as high-order modelling when dealing with moderately thick panels. The discrepancies between the LW models with or without transverse normal strains are mainly justified by the fact the latter assume: (i) plane stress constitutive equations; and (ii) aerodynamic loads applied to the mid-plane transverse displacement (which is constant through-thickness). On the contrary, the LW models based on Lagrange $z$-expansions allow thickness stretching to be captured, while applying the aerodynamic pressure at the very upper surface of the panel, which is exposed to the airflow.

### 4.2. Sandwich panels with viscoelastic core

Regarding the analysis of viscoelastic sandwich panels, the benchmark cases proposed here are based on a well-known test case, widely investigated in the literature. In fact, the original test case also investigated by Araújo et al. [19], Ferreira et al. [24] and Filippi et al. [27] regarding sandwich plates, with constant viscoelastic core loss factor, consists of a thin rectangular panel with sides $a = 348$ mm and $b = 304.8$ mm and total thickness $h = h_0 = 1.778$ mm (each skin with $h_s = 6h/7 = 0.762$ mm and a core with $h_c = h/7 = 0.254$ mm). The material properties of the skins, as an (isotropic) aluminium alloy, are $E = 68.9$ GPa, $\nu = 0.3$ and $\rho = 2740$ kg/m³, whereas the material properties of the core, as an (isotropic) polymer described by a constant viscoelastic model, are $E = 2.67008(1 + i\eta_c)$ MPa, $\eta_c = 0.5$, $\nu = 0.49$ and $\rho = 999$ kg/m³. To extend this well-known test case, it is considered two novel configurations of viscoelastic sandwich panels with skins of laminated composite using unidirectional fibre-reinforced layers, as in a cross-ply laminate, or instead, curvilinear fibre-reinforced composite layers. Furthermore, both thin panels with total thickness $h = h_0$ ($a/h \approx 196$) and moderately thick panels with $h = 4h_0$ ($a/h \approx 49$) are investigated. In addition to the original narrow core configuration with thickness ratio $h_c/h = 1/7$, a new configuration featuring a wide viscoelastic core with thickness

**Table 2**

Convergence analysis results of the LW Lag3 model — first six natural frequencies $f_n$ (Hz) and damping factors $g_n$, besides the flutter pressure parameter $\tilde{\lambda}_F$ of thin viscoelastic sandwich panels with (<0,45>/<−45,−60>/<0,45>) composite skins ($h = h_0$, $h_c/h = 1/7$ and $\eta_c = 0.5$).

| B.C. | Mesh | $f_1$ | $g_1$ (%) | $f_2$ | $g_2$ (%) | $f_3$ | $g_3$ (%) | $f_4$ | $g_4$ (%) | $f_5$ | $g_5$ (%) | $f_6$ | $g_6$ (%) | $\tilde{\lambda}_F$ |
|---|---|---|---|---|---|---|---|---|---|---|---|---|---|---|
| SSSS | $6 \times 6$ | 72.756 | 20.17 | 130.343 | 24.36 | 154.956 | 19.32 | 201.314 | 25.66 | 209.853 | 21.75 | 272.085 | 24.16 | 231.32 |
| | $8 \times 8$ | 72.709 | 20.22 | 130.199 | 24.36 | 154.643 | 19.38 | 200.803 | 25.79 | 209.056 | 21.72 | 271.049 | 24.33 | 231.34 |
| | $10 \times 10$ | 72.683 | 20.24 | 130.144 | 24.37 | 154.518 | 19.41 | 200.646 | 25.82 | 208.775 | 21.73 | 270.737 | 24.38 | 231.34 |
| | $12 \times 12$ | 72.666 | 20.26 | 130.115 | 24.37 | 154.452 | 19.43 | 200.584 | 25.83 | 208.640 | 21.75 | 270.612 | 24.40 | 231.33 |
| | $14 \times 14$ | 72.654 | 20.27 | 130.098 | 24.37 | 154.410 | 19.45 | 200.554 | 25.83 | 208.561 | 21.77 | 270.552 | 24.41 | 231.31 |
| CCCC | $6 \times 6$ | 96.341 | 20.71 | 155.371 | 23.57 | 193.451 | 15.86 | 231.836 | 24.19 | 247.870 | 18.16 | 312.169 | 21.61 | 335.41 |
| | $8 \times 8$ | 96.177 | 20.72 | 154.988 | 23.59 | 192.298 | 15.96 | 230.282 | 24.33 | 246.189 | 18.26 | 309.011 | 22.05 | 334.16 |
| | $10 \times 10$ | 96.113 | 20.72 | 154.856 | 23.59 | 191.939 | 15.99 | 229.831 | 24.37 | 245.675 | 18.30 | 308.093 | 22.18 | 333.78 |
| | $12 \times 12$ | 96.080 | 20.72 | 154.792 | 23.59 | 191.791 | 16.01 | 229.648 | 24.38 | 245.463 | 18.31 | 307.735 | 22.23 | 333.61 |
| | $14 \times 14$ | 96.061 | 20.72 | 154.755 | 23.60 | 191.719 | 16.01 | 229.555 | 24.39 | 245.357 | 18.32 | 307.563 | 22.26 | 333.51 |

ratio $h_c/h = 8/10$ is also investigated. The complete stacking sequences of the symmetric sandwich panels with viscoelastic core are the following:

- *Isotropic aluminium skins*: ($Al$/core/$Al$)
- *Straight fibre composite skins*: (0/90/0/core/0/90/0)
- *Curvilinear fibre composite skins*: (<0,45>/<−45,−60>/<0,45>/core/<0,45>/<−45,−60>/<0,45>)

In the case of laminated composite skins, the layers are of equal thickness and are all made of graphite-epoxy with the following material properties: $E_1 = 173$ GPa, $E_2 = E_3 = 7.20$ GPa, $G_{12} = G_{13} = G_{23} = 3.76$ GPa, $\nu_{12} = \nu_{13} = \nu_{23} = 0.29$ and $\rho = 1540$ kg/m$^3$ [6]. To provide a consistent benchmark, the flutter dynamic pressure parameters are nondimensionalized according to Eq. (17) with $G_0 = 3.76$ GPa, even when considering metal skins. The natural frequencies are now provided in Hz, as $f_n = \omega_n/(2\pi)$, where $n$ stands for the order of the mode, with the corresponding damping factors given as $g_n(\%) = 100g_n$.

Firstly, Table 2 presents the convergence analysis results, including the first six natural frequencies and damping factors (in vacuum) as well as the nondimensionalized flutter dynamic pressure parameters of thin rectangular sandwich panels ($h = h_0$), with narrow viscoelastic core ($h_c/h = 1/7$), along with curvilinear fibre composite skins, considering either simply supported (SSSS) or clamped (CCCC) boundary conditions. For brevity, only the most refined model (LW Lag3) is considered in the present convergence study since a similar convergence behaviour is obtained when making use of the remaining kinematic models.

Comparing the numerical results given in Table 2, the natural frequencies and damping factors of the high-order modes, as well as the nondimensionalized dynamic flutter pressure parameters, start to converge for meshes with more than $10 \times 10$ elements. Even though not shown, it is worth mentioning that the convergence of the natural mode shapes is also ensured, as necessary, considering either free vibrations in vacuum or under the effect of supersonic airflow. It can also be pointed out that as the mesh is increasingly refined: (i) the natural frequencies decrease (as expected), but the damping factors have an increasing trend; and (ii) the flutter pressure parameters mostly tend to decrease. As discussed later on, for both sandwich panels whichever the skins and both boundary conditions, the inclusion of viscoelastic damping leads to the occurrence of single mode flutter, which occurs, in particular, due to the first natural vibration mode.

Since the stiffness matrix associated to the viscoelastic sandwich panels is complex, which increases the computational effort of extracting the eigenvalues compared to a (pure) real matrix, the most refined mesh with $14 \times 14$ elements is not used throughout (as opposed to the cases in Section 4.1). Instead, it is considered the mesh with $10 \times 10$ elements for the following flutter analyses, ensuring the necessary numerical accuracy, while maintaining fast and computationally efficient flutter solutions. By adopting the same FE mesh, the models accuracy assessment is focused on the refinements introduced in the through-thickness distributions of the displacements. Nevertheless, it is worth noting that kinematic models with high-order $z$-expansions of the displacements lead to the same accuracy with a lower number of elements, as compared to formulations with linear $z$-expansions (thus improvements in terms of computational efficiency may occur depending on the number of DOFs involved in the models as well as on the test case).

However, to be consistent with Ferreira et al. [24], the free vibration solutions provided in Table 3 are obtained using a mesh with $12 \times 12$ elements Q9. Specifically, Table 3 presents a verification of the present models predictive capabilities by comparison with the free vibrations solutions reported by Ferreira et al. [24] (LW model adopting linear Lagrange $z$-expansions, within CUF framework), Filippi et al. [27] (LW model with fourth-order $z$-expansions, also within CUF) and Araújo et al. [19] (LW model adopting FSDT for the skins and TSDT for the viscoelastic core), considering the original test case regarding a thin viscoelastic sandwich panel with metal skins. Note that Filippi et al. [27] depending on simply supported or clamped boundary conditions, applied either $10 \times 10$ or $20 \times 20$ elements Q9, respectively, whereas Araújo et al. [19] investigated only clamped plates, applying $12 \times 12$ eight-node serendipity elements (Q8).

A close examination of the numerical results given in Table 3 reveals that:

- ESL descriptions provide rather deficient estimations on accounting for the soft viscoelastic core, predicting highly overestimated natural frequencies and nearly null damping factors (around $10^{-5}\%$). This may be explained by the fact that the ESL models are unable to provide an accurate description of the sandwich panel equivalent properties, as a sole layer/panel, as well as its transverse shear behaviour, namely within the soft viscoelastic core. On the contrary, the proposed LW models

**Table 3**

First six natural frequencies $f_n$ (Hz) and damping factors $g_n$ (%) of thin viscoelastic sandwich panels with aluminium skins ($h = h_0$, $h_c/h = 1/7$ and $\eta_c = 0.5$).

| B.C. | Model | $f_1$ | $g_1$ (%) | $f_2$ | $g_2$ (%) | $f_3$ | $g_3$ (%) | $f_4$ | $g_4$ (%) | $f_5$ | $g_5$ (%) | $f_6$ | $g_6$ (%) |
|------|-------|-------|-----------|-------|-----------|-------|-----------|-------|-----------|-------|-----------|-------|-----------|
| SSSS | Ferreira et al. [24] | 58.608 | 18.52 | 112.254 | 20.49 | 127.001 | 20.20 | 173.418 | 18.60 | 189.834 | 17.95 | 225.704 | 16.58 |
|      | Filippi et al. [27] | 60.236 | 19.00 | 115.240 | 20.30 | 130.450 | 19.90 | 178.500 | 18.10 | 195.620 | 17.40 | 232.950 | 15.90 |
|      | FSDT | 84.410 | 0.00 | 194.328 | 0.00 | 227.688 | 0.00 | 337.556 | 0.00 | 377.635 | 0.00 | 466.597 | 0.00 |
|      | TSDT | 84.408 | 0.00 | 194.320 | 0.00 | 227.676 | 0.00 | 337.531 | 0.00 | 377.604 | 0.00 | 466.550 | 0.00 |
|      | LW FSDT | 60.236 | 19.01 | 115.232 | 20.34 | 130.437 | 19.92 | 178.477 | 18.06 | 195.517 | 17.36 | 232.818 | 15.91 |
|      | LW F/T/F | 60.236 | 19.01 | 115.232 | 20.34 | 130.437 | 19.92 | 178.477 | 18.06 | 195.517 | 17.36 | 232.818 | 15.91 |
|      | LW TSDT | 60.236 | 19.01 | 115.232 | 20.34 | 130.436 | 19.92 | 178.475 | 18.06 | 195.515 | 17.36 | 232.816 | 15.91 |
|      | LW Lag1 | 62.302 | 17.77 | 120.916 | 18.47 | 137.320 | 17.97 | 189.488 | 16.02 | 208.083 | 15.33 | 248.894 | 13.92 |
|      | LW Lag1[a] | 58.608 | 18.52 | 112.254 | 20.49 | 127.001 | 20.20 | 173.418 | 18.60 | 189.834 | 17.95 | 225.704 | 16.58 |
|      | LW Lag2 | 60.236 | 19.01 | 115.232 | 20.34 | 130.437 | 19.92 | 178.476 | 18.06 | 195.518 | 17.36 | 232.819 | 15.91 |
|      | LW Lag3 | 60.236 | 19.01 | 115.232 | 20.34 | 130.437 | 19.92 | 178.475 | 18.06 | 195.517 | 17.36 | 232.817 | 15.91 |
| CCCC | Araújo et al. [19] | 87.660 | 18.86 | 150.100 | 16.30 | 170.990 | 15.27 | 229.070 | 13.42 | 243.790 | 13.23 | 292.210 | 11.79 |
|      | Ferreira et al. [24] | 85.051 | 19.24 | 144.553 | 17.04 | 164.695 | 16.01 | 216.561 | 14.59 | 233.159 | 14.13 | 279.971 | 12.60 |
|      | Filippi et al. [27] | 87.719 | 18.90 | 149.480 | 16.40 | 170.540 | 15.40 | 224.590 | 13.90 | 241.850 | 13.40 | 290.870 | 11.90 |
|      | FSDT | 154.56 | 0.00 | 289.241 | 0.00 | 339.454 | 0.00 | 463.613 | 0.00 | 504.589 | 0.00 | 624.442 | 0.00 |
|      | TSDT | 154.55 | 0.00 | 289.208 | 0.00 | 339.410 | 0.00 | 463.534 | 0.00 | 504.503 | 0.00 | 624.313 | 0.00 |
|      | LW FSDT | 87.399 | 18.94 | 148.935 | 16.48 | 169.907 | 15.40 | 223.751 | 13.91 | 241.071 | 13.46 | 289.942 | 11.93 |
|      | LW F/T/F | 87.399 | 18.94 | 148.935 | 16.48 | 169.907 | 15.40 | 223.751 | 13.91 | 241.071 | 13.46 | 289.942 | 11.93 |
|      | LW TSDT | 87.398 | 18.94 | 148.933 | 16.48 | 169.904 | 15.40 | 223.747 | 13.91 | 241.066 | 13.46 | 289.935 | 11.93 |
|      | LW Lag1 | 92.217 | 17.14 | 158.669 | 14.58 | 181.620 | 13.53 | 240.276 | 12.10 | 259.214 | 11.67 | 312.990 | 10.26 |
|      | LW Lag1[a] | 85.051 | 19.24 | 144.553 | 17.04 | 164.695 | 16.01 | 216.561 | 14.59 | 233.159 | 14.13 | 279.971 | 12.60 |
|      | LW Lag2 | 87.924 | 18.90 | 149.851 | 16.41 | 170.980 | 15.33 | 225.148 | 13.84 | 242.612 | 13.38 | 291.859 | 11.86 |
|      | LW Lag3 | 87.923 | 18.90 | 149.849 | 16.41 | 170.978 | 15.33 | 225.144 | 13.84 | 242.608 | 13.38 | 291.852 | 11.86 |

[a] $\nu_{12} = \nu_{13} = \nu_{23} = 0$ for the face layers (as in [24]).

predict very coherent results, in agreement with the benchmark solutions [19,24,27], which further corroborate that LW type descriptions are mandatory for proper modelling and analysis of viscoelastic sandwich panels with high inhomogeneity of material properties through-thickness. Therefore, ESL descriptions are not considered in any further analyses of viscoelastic sandwich panels.

- Since the proposed LW shear deformation models are in good agreement with each other, it is concluded that the use of third-order theories – either for the core alone or for both core and skins – adds no significant advantage in the evaluation of the first six natural frequencies and damping factors in this test case.
- In comparison to the remaining models, the LW Lag1 model overpredicts the natural frequencies and underpredicts the damping factors due to thickness locking. If one assumes null Poisson ratio for the metal skins to alleviate thickness locking, the LW Lag1 model underestimates the natural frequencies and overestimates the damping factors in comparison to the high-order models (which are insensitive to thickness locking [56]). Since Ferreira et al. [24] also considered a LW linear Lagrange model, applying the same FE mesh, it is observed that the present results coincide with [24] if one assumes null Poisson ratio, as also discussed in the assessment provided by Liu et al. [25]. Overall, the use of at least quadratic Lagrange $z$-expansions ($N = 2$) appears rather necessary to obtain accurate solutions, without modifying the 3D constitutive equations.
- The use of LW FSDT with reduced plane stress constitutive equations provides solutions closer to the quasi-3D models than the LW Lag1 model, while using a lower number of DOFs.
- In the present test case, the LW Lag3 model (with a cubic Lagrange $z$-expansion) adds no significant advantage over the LW Lag2 model (with a quadratic Lagrange $z$-expansion). In fact, both models are in good agreement with the solutions reported by Filippi et al. [27], making use of a LW model with a fourth-order $z$-expansion, noting that the discrepancies are mainly due to different discretization levels in-plane since the present results are obtained with $12 \times 12$ elements, whereas in [27], depending on simply supported or clamped boundary conditions, it is considered either $10 \times 10$ or $20 \times 20$ elements, respectively.
- The LW models that account for transverse normal deformations tend to predict slightly higher natural frequencies and lower damping factors than the models which neglect thickness stretching, while assuming a plane stress state, especially in the case of clamped plates.

In terms of the aeroelastic analysis, Table 4 presents the nondimensionalized flutter pressure parameters of the viscoelastic sandwich panels with core loss factor $\eta_c = 0.5$, alongside the relative discrepancy of each kinematic model to the most refined model (LW Lag3). Firstly, it is worth underlying that as a result of the viscoelastic core, single mode flutter occurs for all sandwich panels whichever the skins, with both simply supported and clamped boundary conditions, as perceived from Fig. 3. In fact, Fig. 4 further highlights the influence of the core loss factor on the decoupling of the modes, in line with thin or moderately thick panels. Specifically, for a null core loss factor ($\eta_c = 0$), i.e. a purely elastic core, flutter clearly occurs due to the first two modes coalescence, which is characterized by a complex conjugated pair, where natural frequencies merge together and damping factors are symmetric. On the other hand, for a viscoelastic core ($\eta_c = 0.5$), the eigenvalues do not emerge as complex conjugated pairs at the flutter bound and, therefore, neither natural frequencies coalescence occurs nor symmetric damping factors are exhibited. As represented in both Figs. 3 and 4, single mode flutter due to the first vibration mode does occur since its damping factor turns from positive to negative,

**Table 4**
Flutter dynamic pressure parameters $\tilde{\lambda}_F$ of viscoelastic sandwich panels ($\eta_c = 0.5$), with metal or composite skins, considering thin and moderately thick panels, with either narrow ($h_c/h = 1/7$) or wide core ($h_c/h = 8/10$).

| B.C. | $h_c/h$ | Model | Aluminium skins | | | | (0/90/0) skins | | | | (<0,45>/<−45,−60>/<0,45>) skins | | | |
|---|---|---|---|---|---|---|---|---|---|---|---|---|---|---|
| | | | $h = h_0$[a] | $\delta(\%)$ | $h = 4h_0$[b] | $\delta(\%)$ | $h = h_0$[a] | $\delta(\%)$ | $h = 4h_0$[b] | $\delta(\%)$ | $h = h_0$[a] | $\delta(\%)$ | $h = 4h_0$[b] | $\delta(\%)$ |
| SSSS | 1/7 | LW FSDT | 235.26 | 0.000 | 138.06 | −0.094 | 231.61 | 0.004 | 187.26 | −0.021 | 231.48 | 0.061 | 105.44 | 0.038 |
| | | LW F/T/F | 235.26 | 0.000 | 138.06 | −0.094 | 231.61 | 0.004 | 187.26 | −0.021 | 231.48 | 0.061 | 105.44 | 0.038 |
| | | LW TSDT | 235.26 | 0.000 | 138.04 | −0.109 | 231.59 | −0.004 | 187.00 | −0.160 | 231.30 | −0.017 | 105.32 | −0.076 |
| | | LW Lag1 | 258.10 | 9.708 | 166.97 | 20.83 | 232.80 | 0.518 | 189.18 | 1.004 | 232.88 | 0.666 | 108.50 | 2.941 |
| | | LW Lag2 | 235.26 | 0.000 | 138.21 | 0.014 | 231.61 | 0.004 | 187.55 | 0.133 | 231.36 | 0.009 | 105.50 | 0.095 |
| | | LW Lag3 | 235.26 | | 138.19 | | 231.60 | | 187.30 | | 231.34 | | 105.40 | |
| | 8/10 | LW FSDT | 67.239 | −0.001 | 7.441 | −0.013 | 56.024 | −0.002 | 7.722 | −0.013 | 63.709 | 0.039 | 7.307 | −0.014 |
| | | LW F/T/F | 67.239 | −0.001 | 7.441 | −0.013 | 56.024 | −0.002 | 7.722 | −0.013 | 63.709 | 0.039 | 7.307 | −0.014 |
| | | LW TSDT | 67.239 | −0.001 | 7.441 | −0.013 | 56.024 | −0.002 | 7.722 | −0.013 | 63.676 | −0.013 | 7.307 | −0.014 |
| | | LW Lag1 | 67.562 | 0.479 | 7.766 | 4.354 | 56.078 | 0.095 | 7.743 | 0.259 | 63.758 | 0.116 | 7.329 | 0.287 |
| | | LW Lag2 | 67.240 | 0.000 | 7.442 | 0.000 | 56.025 | 0.000 | 7.723 | 0.000 | 63.685 | 0.002 | 7.308 | 0.000 |
| | | LW Lag3 | 67.240 | | 7.442 | | 56.025 | | 7.723 | | 63.684 | | 7.308 | |
| CCCC | 1/7 | LW FSDT | 355.29 | −0.981 | 217.15 | −1.524 | 451.13 | −0.033 | 331.82 | −0.141 | 333.43 | −0.105 | 163.15 | −0.092 |
| | | LW F/T/F | 355.29 | −0.981 | 217.15 | −1.524 | 451.13 | −0.033 | 331.82 | −0.141 | 333.43 | −0.105 | 163.15 | −0.092 |
| | | LW TSDT | 355.28 | −0.984 | 217.05 | −1.569 | 451.02 | −0.058 | 330.36 | −0.581 | 333.36 | −0.126 | 162.75 | −0.337 |
| | | LW Lag1 | 399.01 | 11.20 | 264.50 | 19.95 | 453.83 | 0.565 | 336.21 | 1.180 | 336.09 | 0.692 | 168.64 | 3.270 |
| | | LW Lag2 | 358.82 | 0.003 | 220.61 | 0.045 | 451.37 | 0.020 | 333.74 | 0.436 | 333.83 | 0.015 | 163.68 | 0.233 |
| | | LW Lag3 | 358.81 | | 220.51 | | 451.28 | | 332.29 | | 333.78 | | 163.30 | |
| | 8/10 | LW FSDT | 80.439 | −0.344 | 8.438 | −0.624 | 80.342 | −0.025 | 9.379 | −0.053 | 75.485 | −0.048 | 8.307 | −0.096 |
| | | LW F/T/F | 80.439 | −0.344 | 8.438 | −0.624 | 80.342 | −0.025 | 9.379 | −0.053 | 75.485 | −0.048 | 8.307 | −0.096 |
| | | LW TSDT | 80.439 | −0.344 | 8.438 | −0.624 | 80.340 | −0.027 | 9.377 | −0.075 | 75.483 | −0.050 | 8.307 | −0.096 |
| | | LW Lag1 | 81.178 | 0.571 | 8.958 | 5.500 | 80.396 | 0.042 | 9.420 | 0.384 | 75.563 | 0.056 | 8.348 | 0.397 |
| | | LW Lag2 | 80.717 | 0.000 | 8.491 | 0.000 | 80.365 | 0.004 | 9.385 | 0.011 | 75.523 | 0.003 | 8.316 | 0.012 |
| | | LW Lag3 | 80.717 | | 8.491 | | 80.362 | | 9.384 | | 75.521 | | 8.315 | |

$\delta(\%) = (\tilde{\lambda}_F - \tilde{\lambda}_F^{\text{LW Lag3}}) \times 100/\tilde{\lambda}_F^{\text{LW Lag3}}$.

[a] $a/h \approx 196$.

[b] $a/h \approx 49$.

with no merging of natural frequencies. Moreover, the damping factors associated to the high-order modes can decrease, increase or remain almost constant as the dynamic pressure parameter increases, but remaining quite further above the unstable zone ($g < 0$) around the flutter bound. Throughout Figs. 3 and 4, the evolution of the natural frequencies and damping factors is presented using the LW Lag3 and LW FSDT/TSDT/FSDT models, which are shown to be in good agreement.

Regarding the analysis of sandwich panels with variable stiffness composite skins and a core thickness ratio either narrow $h_c/h = 1/7$ or wide $h_c/h = 8/10$, as shown in the right-hand side of Fig. 3 and in the top right-corner of Fig. 4, respectively, it is understood that in the case of a wide core: (i) the natural frequencies decrease; (ii) the damping factors increase; and (iii) the flutter pressure parameter decreases. Besides the fact that the flutter bound decreases when considering a wide core, it is also perceived that as the dynamic pressure parameter increases all damping factors show a rather pronounced decreasing trend and the third mode can also be aeroelastically unstable at a higher dynamic pressure parameter.

In terms of the models accuracy assessment, the numerical results provided in Table 4 reveal that in the case of simply supported panels, the LW shear deformation models mostly underpredict the flutter pressure parameters in comparison to the LW models based on Lagrange $z$-expansions of high-order ($N = 2$ or $3$) with thickness stretching. Nevertheless, the discrepancies between these models are quite small, which further highlights the ideal capability of the LW FSDT model to render both computationally efficient and numerically accurate aeroelastic solutions. In fact, the discrepancies between the LW shear deformation models and the LW high-order Lagrange $z$-expansion models, with quasi-3D predictive capabilities, are higher for clamped boundary conditions than for simply supported. To be precise, for clamped plates, the LW shear deformation models underestimate the flutter bounds as compared to the LW Lag2 and LW Lag3 models, noting that the higher discrepancies are found for the case of aluminium skins (around 1%), whereas for the composite skins, the respective discrepancies are considerably lower. Comparing the two sandwich panels with composite skins, it is noticed that the discrepancies tend to be higher for the curvilinear fibre composite skins, which exhibit high flexural anisotropy, involving bending–twisting coupling.

Additionally, for the test cases presented in Table 4, there is no difference between the results obtained using the full LW FSDT and the LW FSDT/TSDT/FSDT models. Inspecting the solutions obtained using the LW TSDT model, it is also concluded that there is no major advantage of assuming a cubic (rather than linear) distribution of in-plane displacements, especially when dealing with metal skins. Another important aspect to note is that the flutter bounds predicted by the LW Lag1 model are always overestimated, as compared to the remaining models. The thickness locking in the LW Lag1 model is particularly relevant in the case of metal skins, where discrepancies around 20% are verified when considering moderately thick panels with narrow core. These discrepancies are in line with the fact that thickness locking in orthotropic and laminated plates is significantly reduced as compared to the case of
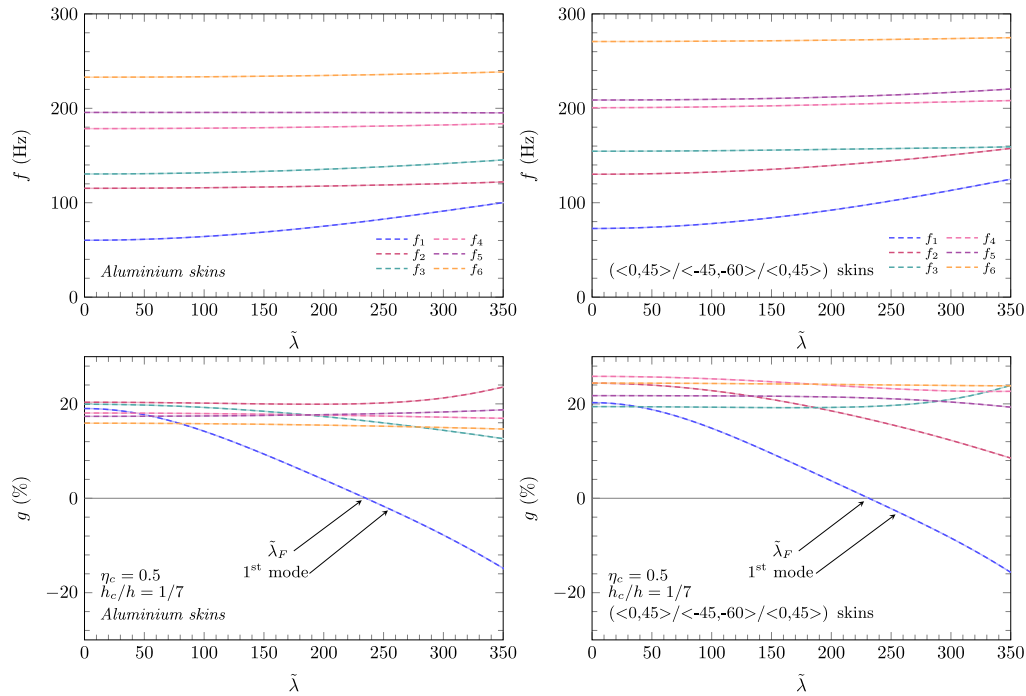
**Fig. 3.** Variation of the first six natural frequencies $f_n$ and damping factors $g_n$ with the nondimensionalized pressure parameter $\tilde{\lambda}$ of simply supported viscoelastic sandwich panels, with $h = h_0$ and narrow core ($h_c/h = 1/7$ and $\eta_c = 0.5$): LW Lag3 (solid lines) and LW F/T/F (dashed lines) models.

pure isotropic plates, as discussed in detail by Carrera and Brischetto [56]. As a result, it is emphasized the mandatory mitigation of thickness locking effects in models with constant distribution of transverse normal strains in order to obtain accurate panel flutter solutions. This is attainable by assuming, for instance, either high-order theory for the transverse displacement (e.g., LW Lag2) or reduced plane stress constitutive equations (e.g., LW shear deformation models). A close examination of the results provided in Table 4, concerning the LW high-order Lagrange $z$-expansion models, leads to the conclusion that converged solutions can be obtained, from a purely practical point of view, when making use of quadratic $z$-expansions, especially for thin panels with $h = h_0$. Nonetheless, for moderately thick panels with $h = 4h_0$ and narrow core $h_c/h = 1/7$, there are some slight discrepancies between the LW Lag2 and LW Lag3 models in the case of composite skins.

In the case of sandwich panels with a viscoelastic core having a temperature-dependent behaviour [58], the discrepancies between the different kinematic models may increase or decrease depending on the properties of the viscoelastic material for a given range of temperatures, as well as on the difference between the properties of the core and the properties of the skins. Nonetheless, for sandwich panels with softer viscoelastic cores (arising, for instance, due to increases in the operational temperature), the transverse shear deformations and thickness stretching are expected to contribute more to the aeroelastic response. Hence, the application of high-order theories with thickness stretching is indeed relevant to obtain accurate aeroelastic solutions when dealing with soft core sandwich panels under non-isothermal conditions, involving viscoelastic materials with a pronounced temperature-dependent behaviour.

To provide a complete understanding on the aeroelastic response behaviour of supersonic viscoelastic sandwich panels, exploring the combined application of a viscoelastic damping core along with curvilinear fibre composite skins, Fig. 5 shows the evolution of the flutter pressure parameters with the core thickness ratio ($h_c/h$ from 0.05 to 0.8) of thin viscoelastic sandwich panels ($h = h_0$), considering five distinct core loss factors, viz. $\eta_c = 0$ (purely elastic core) and $\eta_c = 0.5$, 1, 2 and 5, as well as both simply supported and clamped boundary conditions. Even though not shown, for brevity, the results for $\eta_c = 0.1$ and 0.01 are just slightly below the curves associated to $\eta_c = 0.5$. In this assessment, it is used the LW FSDT/TSDT/FSDT model as well as the LW model with cubic Lagrange $z$-expansions. Actually, Fig. 5 attests once more the good agreement between the two kinematic models, underlying that thickness stretching plays a minor role in the flutter behaviour of thin sandwich panels in supersonic airflow, whether the core is purely elastic or viscoelastic at some degree, as perceived from the overlapped lines. This conclusion holds equally regardless of the type of skins and core thickness ratio, as well as for both simply supported and clamped boundary conditions. Moreover, for the case of purely elastic core ($\eta_c = 0$), it is verified that all sandwich panels exhibit mode coalescence as flutter occurs due to the first two modes (as shown in Fig. 4 for the particular case of $h_c/h = 8/10$), whereas for the case of (any) viscoelastic core, it is found single mode flutter due to the first vibration mode, regardless of the core thickness ratio and boundary conditions.

As observed in Fig. 5, the flutter dynamic pressure parameters tend to decrease as the core becomes thicker due to a loss in the overall stiffness of the sandwich panels. Moreover, the introduction of low viscoelastic damping tends to have a disadvantageous
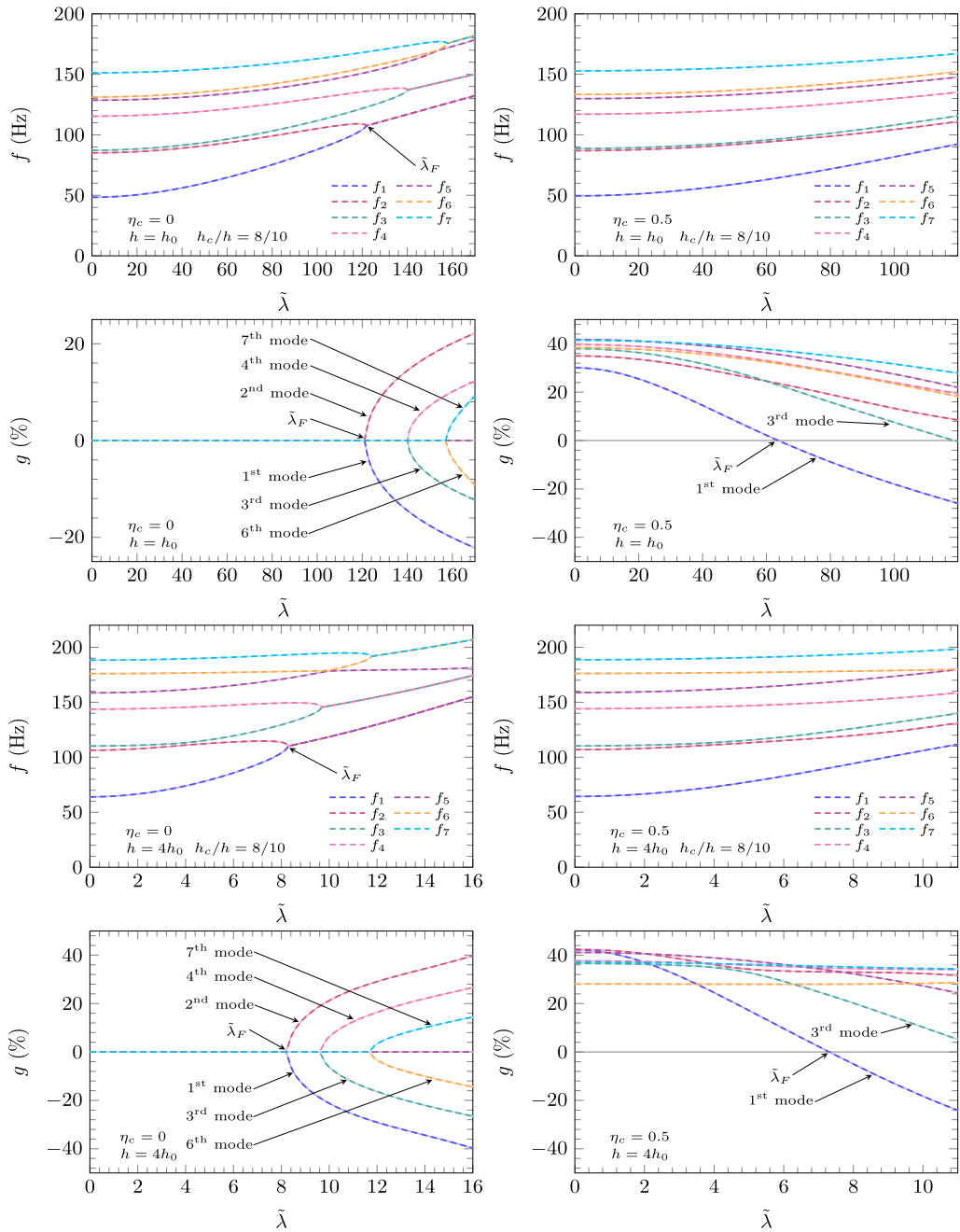
**Fig. 4.** Variation of the first seven natural frequencies $f_n$ and damping factors $g_n$ with the nondimensionalized pressure parameter $\tilde{\lambda}$ of simply supported sandwich panels, with (<0,45>/<−45,−60>/<0,45>) composite skins and core thickness ratio $h_c/h = 8/10$: LW Lag3 (solid lines) and LW F/T/F (dashed lines) models.

effect on the flutter resistance of sandwich panels of narrow core, as compared to a purely elastic core, especially in the case of simply supported boundary conditions. Nonetheless, as the core loss factor increases, the curves tend to move upwards, i.e. the flutter bounds increase, and can even surpass the case of purely elastic core for some core thickness ratios (thus suggesting that viscoelastic damping has indeed potential for the aeroelastic stability augmentation in supersonic sandwich panels). In fact, when considering $\eta_c = 5$, higher flutter bounds are found compared to $\eta_c = 0$ or 2, for most core thickness ratios and for both simply supported and clamped boundary conditions. The results regarding the higher material loss factor of the core $\eta_c = 5$ have a slightly different trend in the case of simply supported boundary conditions. This behaviour may be explained not only by the combined effect of the boundary conditions and the type of skins, but also by the high core loss factor. In fact, the assumed core loss factor of $\eta_c = 5$ is ten times higher than the value considered in the original test case ($\eta_c = 0.5$) and, therefore, the contribution of the
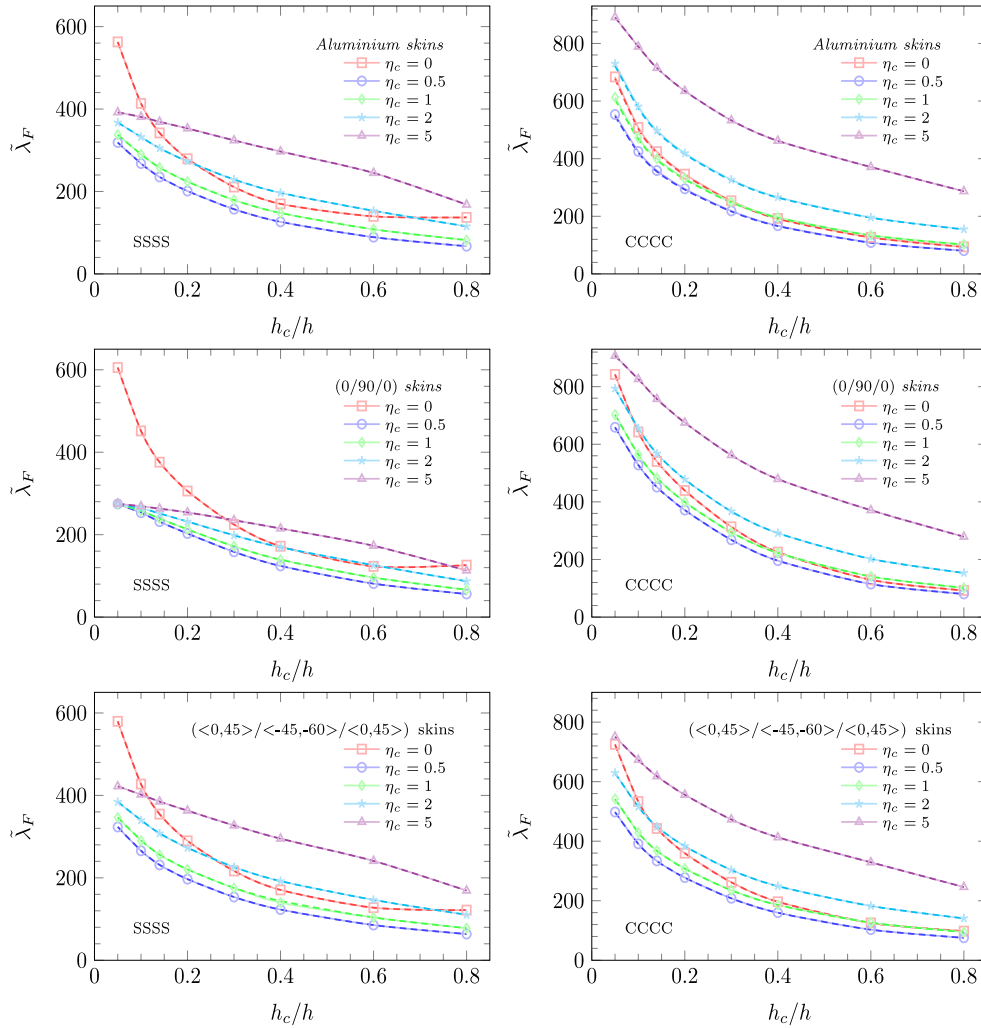
**Fig. 5.** Evolution of the flutter pressure parameters $\tilde{\lambda}_F$ with the core thickness ratio $h_c/h$ of thin viscoelastic sandwich panels, considering various core loss factors $\eta_c$: LW F/T/F (dashed line) and LW Lag3 (solid line) models.

material damping to the aeroelastic response increases significantly (noting that the added damping is further pronounced as the core thickness ratio increases).

For clamped sandwich panels, the use of lower core loss factors, such as $\eta_c = 1$ or 0.5, can match or surpass the results without viscoelastic damping, but only when considering quite wide cores, whereas the curves associated to $\eta_c = 2$ are mostly above the case of purely elastic core, even for relatively low core thickness ratios. As regards to simply supported panels, the benefits of the viscoelastic damping are more subtle, being particularly noticed for sandwich panels with high core loss factor ($\eta_c \geq 2$).

Comparing the different sandwich panels in terms of aeroelastic stability, the present variable stiffness composite skins do not add any significant improvement over the conventional cross-ply or metal skins when clamped boundary conditions are considered. On the contrary, for simply supported panels, rather considerable flutter improvements can be found when comparing sandwich panels with curvilinear fibre composite skins as opposed to the more conventional cross-ply composite skins. In addition, it is interesting to note that for simply supported viscoelastic sandwich panels with cross-ply composite skins, there is no major differences in the flutter bounds of the panels with narrow core, whereas in the remaining cases, a clear distinction among the curves can be perceived.

In effect, for simply supported panels, the improvements in terms of flutter bound brought to light by the use of composite skins reinforced by curvilinear fibres instead of unidirectional fibres depend not only on the core thickness ratio but also on the core loss factor. For example, when considering $\eta_c = 0.5$, it is observed an increase of flutter pressure parameter, as an improvement, around 18% and 14% for $h_c/h = 0.05$ and 0.80, respectively, whereas for $h_c/h = 0.10$ and 0.60, it is just 5%. For $\eta_c = 1$, 2 and 5, the maximum improvements occur for $h_c/h = 0.05$, around 26%, 40% and 53%, each, while the minimum happen for $h_c/h = 0.40$, around 1%, 13% and 37%, respectively. Moreover, for $\eta_c = 5$ and $h_c/h = 0.80$, there is also a remarkable increase of 50% in the flutter bound when comparing composite skins using curvilinear fibres instead of unidirectional fibres.

All in all, the results shown in Fig. 5 and the conclusions outlined emphasize the need for aeroelastic design optimization of viscoelastic sandwich panels to obtain improved dynamic and aeroelastic characteristics, which can be further enhanced by careful tailoring of curvilinear fibre composite skins. Moreover, in real aerospace applications, the inclusion of temperature effects – such as thermal loads and temperature-dependent viscoelastic materials – is quite relevant to completely describe the actual aero-thermo-viscoelastic behaviour of supersonic sandwich panels with soft viscoelastic core [34,37,39] and it must be considered, along with previously mentioned design parameters, for proper aeroelastic design optimization.

## 5. Conclusions

In light of the proper modelling of soft core sandwich panels with viscoelastic damping, most especially, under supersonic airflow, this work discusses the role of structural kinematic theories on the aeroelastic flutter stability analysis, making progress on the application of highly refined models, with quasi-3D predictive capabilities, while pushing forward on the combined application of a viscoelastic damping core and curvilinear fibre composite skins, as promising structural design technologies, suitable for advanced aerospace structures. An assessment of 2D finite elements is provided, exploring LW kinematic descriptions using either variable-order shear deformation theories or, in general, theories based on Lagrange $z$-expansions with thickness stretching, focusing for the first time on the supersonic panel flutter of viscoelastic sandwich panels with skins of metal or laminated composite, using unidirectional or curvilinear fibres. The proposed models make use of the First-order Piston Theory to obtain the pressure distribution generated by the supersonic airflow as well as the complex modulus approach to describe the behaviour of the viscoelastic core material.

Numerical applications provide a comprehensive assessment of the models predictive capabilities through various illustrative examples, along with a comparison with available literature solutions, including both 3D exact free vibration solutions and refined FE predictions. The aeroelastic response behaviour of sandwich panels is demonstrated and discussed, in terms of the influence of some design parameters, such as the core loss factor and core thickness ratio, as well as the skins material and boundary conditions. In the presented test cases, it is identified mode coalescence as flutter occurs in sandwich panels with purely elastic core, whereas single mode flutter arises in the case of viscoelastic core. Moreover, the introduction of viscoelastic damping can lead to either a stabilizing or destabilizing effect on the flutter bounds, as compared to sandwich panels with purely elastic core, depending on the previously mentioned design parameters.

As far as thin panels are considered, which are of primary interest for most aerospace applications, it is concluded that the LW FSDT model ensures the best compromise between numerical accuracy and computational effort on supersonic flutter analysis of soft core sandwich panels, with either viscoelastic or purely elastic core. In fact, there is no significant improvements when the TSDT is considered for the core alone or even for both core and skins. Nevertheless, it is worth mentioning that for moderately thick panels with relatively low side-to-thickness ratios, LW high-order models accounting for thickness stretching effects appear to be quite necessary to obtain accurate aeroelastic flutter solutions in soft core sandwich panels. In terms of quasi-3D descriptions involving LW Lagrange $z$-expansions for all displacement components, the use of at least quadratic expansions is pointed out as being capable of rendering accurate flutter predictions, without thickness locking (as opposed to first-order expansions). Note that such conclusions are drawn as regards to the linear aeroelastic flutter stability analysis of supersonic sandwich panels and, therefore, may not hold equally when the dynamic response of displacements and, most especially, 3D stresses is required (such as in fatigue and failure analysis).

All in all, this work provides new and complete benchmarks for ensuing research on the aero-visco-elastic panel flutter analysis of supersonic sandwich panels, which may address later on the combined aeroelastic design optimization of viscoelastic soft core and curvilinear fibre composite skins tailoring, all together, to ensure the development of lightweight structures featuring enhanced dynamic and aeroelastic characteristics. Ultimately, to obtain a complete understating of the aeroelastic response behaviour of viscoelastic sandwich panels, the exploration of different types of boundary conditions and airflow directions is important to consider in future works, including not only the variation of the natural frequencies and modal loss factors with the dynamic pressure but also the evolution of the natural mode shapes.

## CRediT authorship contribution statement

**J.A. Moreira:** Conceptualization, Methodology, Software, Validation, Formal analysis, Investigation, Resources, Data curation, Writing – original draft, Writing – review & editing, Visualization, Project administration, Funding acquisition. **F. Moleiro:** Conceptualization, Methodology, Writing – review & editing, Supervision, Project administration, Funding acquisition. **A.L. Araújo:** Conceptualization, Methodology, Writing – review & editing, Supervision, Funding acquisition. **A. Pagani:** Conceptualization, Writing – review & editing, Supervision, Funding acquisition.

## Declaration of competing interest

The authors declare that they have no known competing financial interests or personal relationships that could have appeared to influence the work reported in this paper.

## Data availability

Data will be made available on request.

## Acknowledgements

## References

[1] R.A. DiTaranto, Theory of vibratory bending for elastic and viscoelastic layered finite-length beams, J. Appl. Mech. 32 (4) (1965) 881–886, http://dx.doi.org/10.1115/1.3627330.

[2] D.J. Mead, S. Markus, The forced vibration of a three-layer, damped sandwich beam with arbitrary boundary conditions, J. Sound Vib. 10 (2) (1969) 163–175, http://dx.doi.org/10.1016/0022-460X(69)90193-X.

[3] E. Carrera, Theories and finite elements for multilayered anisotropic, composite plates and shells, Arch. Comput. Methods Eng. 9 (2) (2002) 87–140, http://dx.doi.org/10.1007/BF02736649.

[4] K.M. Liew, Z.Z. Pan, L.W. Zhang, An overview of layerwise theories for composite laminates and structures: Development, numerical implementation and application, Compos. Struct. 216 (2019) 240–259, http://dx.doi.org/10.1016/j.compstruct.2019.02.074.

[5] F. Moleiro, C.M. Mota Soares, E. Carrera, J.N. Reddy, Evaluation of exact electro-elastic static and free vibration solutions of multilayered plates for benchmarking: piezoelectric composite laminates and soft core sandwich plates, Composites C 2 (2020) 100038, http://dx.doi.org/10.1016/j.jcomc.2020.100038.

[6] J.A. Moreira, F. Moleiro, A.L. Araújo, A. Pagani, Assessment of layerwise user-elements in Abaqus for static and free vibration analysis of variable stiffness composite laminates, Compos. Struct. 303 (2023) 116291, http://dx.doi.org/10.1016/j.compstruct.2022.116291.

[7] C.S. Lopes, Z. Gürdal, P.P. Camanho, Variable-stiffness composite panels: Buckling and first-ply failure improvements over straight-fibre laminates, Comput. Struct. 86 (9) (2008) 897–907, http://dx.doi.org/10.1016/j.compstruc.2007.04.016.

[8] O. Stodieck, J.E. Cooper, P.M. Weaver, P. Kealy, Improved aeroelastic tailoring using tow-steered composites, Compos. Struct. 106 (2013) 703–715, http://dx.doi.org/10.1016/j.compstruct.2013.07.023.

[9] O. Stodieck, J.E. Cooper, P.M. Weaver, P. Kealy, Optimization of tow-steered composite wing laminates for aeroelastic tailoring, AIAA J. 53 (8) (2015) 2203–2215, http://dx.doi.org/10.2514/1.J053599.

[10] T.A. Guimarães, S.G. Castro, C.E. Cesnik, D.A. Rade, Supersonic flutter and buckling optimization of tow-steered composite plates, AIAA J. 57 (1) (2019) 397–407, http://dx.doi.org/10.2514/1.J057282.

[11] J. Fazilati, V. Khalafi, Aeroelastic panel flutter optimization of tow-steered variable stiffness composite laminated plates using isogeometric analysis, J. Reinf. Plast. Compos. 38 (19–20) (2019) 885–895, http://dx.doi.org/10.1177/0731684419854800.

[12] J.A. Moreira, F. Moleiro, A.L. Araújo, A. Pagani, Analytical modeling of panel flutter and active control in supersonic variable stiffness composite laminates, Mech. Adv. Mater. Struct. (2022) 1–15, http://dx.doi.org/10.1080/15376494.2022.2144970.

[13] J.S. Moita, A.L. Araújo, P. Martins, C.M. Mota Soares, C.A. Mota Soares, A finite element model for the analysis of viscoelastic sandwich structures, Comput. Struct. 89 (21) (2011) 1874–1881, http://dx.doi.org/10.1016/j.compstruct.2011.05.008.

[14] W. Larbi, J.F. Deü, R. Ohayon, Vibroacoustic analysis of double-wall sandwich panels with viscoelastic core, Comput. Struct. 174 (2016) 92–103, http://dx.doi.org/10.1016/j.compstruc.2015.09.012.

[15] S. Ren, G. Zhao, S. Zhang, A layerwise finite element formulation for vibration and damping analysis of sandwich plate with moderately thick viscoelastic core, Mech. Adv. Mater. Struct. 27 (14) (2020) 1201–1212, http://dx.doi.org/10.1080/15376494.2018.1504360.

[16] P. Cupial, J. Niziol, Vibration and damping analysis of a three-layered composite plate with a viscoelastic mid-layer, J. Sound Vib. 183 (1) (1995) 99–114, http://dx.doi.org/10.1006/jsvi.1995.0241.

[17] R. Rikards, A. Chate, E. Barkanov, Finite element analysis of damping the vibrations of laminated composites, Comput. Struct. 47 (6) (1993) 1005–1015, http://dx.doi.org/10.1016/0045-7949(93)90305-W.

[18] R.A.S. Moreira, J.D. Rodrigues, A.J.M. Ferreira, A generalized layerwise finite element for multi-layer damping treatments, Comput. Mech. 37 (5) (2006) 426–444, http://dx.doi.org/10.1007/s00466-005-0714-1.

[19] A.L. Araújo, C.M. Mota Soares, C.A. Mota Soares, Finite element model for hybrid active-passive damping analysis of anisotropic laminated sandwich structures, J. Sandw. Struct. Mater. 12 (2010) 397–419, http://dx.doi.org/10.1177/1099636209104534.

[20] A.L. Araújo, C.M. Mota Soares, C.A. Mota Soares, J. Herskovits, Optimal design and parameter estimation of frequency dependent viscoelastic laminated sandwich composite plates, Compos. Struct. 92 (9) (2010) 2321–2327, http://dx.doi.org/10.1016/j.compstruct.2009.07.006.

[21] J.S. Moita, A.L. Araújo, C.M. Mota Soares, C.A. Mota Soares, Finite element model for damping optimization of viscoelastic sandwich structures, Adv. Eng. Softw. 66 (2013) 34–39, http://dx.doi.org/10.1016/j.advengsoft.2012.10.002.

[22] T.S. Plagianakos, D.A. Saravanos, High-order layerwise finite element for the damped free-vibration response of thick composite and sandwich composite plates, Internat. J. Numer. Methods Engrg. 77 (11) (2009) 1593–1626, http://dx.doi.org/10.1002/nme.2465.

[23] B.E. Douglas, J.C.S. Yang, Transverse compressional damping in the vibratory response of elastic-viscoelastic-elastic beams, AIAA J. 16 (9) (1978) 925–930, http://dx.doi.org/10.2514/3.7595.

[24] A.J.M. Ferreira, A.L. Araújo, A.M.A. Neves, J.D. Rodrigues, E. Carrera, M. Cinefra, C.M. Mota Soares, A finite element model using a unified formulation for the analysis of viscoelastic sandwich laminates, Composites B 45 (1) (2013) 1258–1264, http://dx.doi.org/10.1016/j.compositesb.2012.05.012.

[25] B. Liu, L. Zhao, A.J.M. Ferreira, Y.F. Xing, A.M.A. Neves, J. Wang, Analysis of viscoelastic sandwich laminates using a unified formulation and a differential quadrature hierarchical finite element method, Composites B 110 (2017) 185–192, http://dx.doi.org/10.1016/j.compositesb.2016.11.028.

[26] M. Filippi, E. Carrera, Various refined theories applied to damped viscoelastic beams and circular rings, Acta Mech. 228 (2017) 4235–4248, http://dx.doi.org/10.1007/s00707-017-1948-7.

[27] M. Filippi, E. Carrera, S. Valvano, Analysis of multilayered structures embedding viscoelastic layers by higher-order, and zig-zag plate elements, Composites B 154 (2018) 77–89, http://dx.doi.org/10.1016/j.compositesb.2018.07.054.

[28] A. Alaimo, C. Orlando, S. Valvano, Analytical frequency response solution for composite plates embedding viscoelastic layers, Aerosp. Sci. Technol. 92 (2019) 429–445, http://dx.doi.org/10.1016/j.ast.2019.06.021.

[29] M. D'Ottavio, A. Krasnobrizha, E. Valot, O. Polit, R. Vescovini, L. Dozio, Dynamic response of viscoelastic multiple-core sandwich structures, J. Sound Vib. 491 (2021) 115753, http://dx.doi.org/10.1016/j.jsv.2020.115753.

[30] V.V. Bolotin, A.A. Grishko, A.V. Petrovsky, Secondary bifurcations and global instability of an aeroelastic non-linear system in the divergence domain, J. Sound Vib. 191 (3) (1996) 431–451, http://dx.doi.org/10.1006/jsvi.1996.0132.

[31] G.A. Oyibo, Unified panel flutter theory with viscous damping effects, AIAA J. 21 (5) (1983) 767–773, http://dx.doi.org/10.2514/3.8145.

[32] K.-N. Koo, W.-S. Hwang, Effects of hysteretic and aerodynamic damping on supersonic panel flutter of composite plates, J. Sound Vib. 273 (3) (2004) 569–583, http://dx.doi.org/10.1016/S0022-460X(03)00514-5.

[33] H. Akhavan, P. Ribeiro, Aeroelasticity of composite plates with curvilinear fibres in supersonic flow, Compos. Struct. 194 (2018) 335–344, http://dx.doi.org/10.1016/j.compstruct.2018.03.101.

[34] A.G. Cunha-Filho, A.M.G. de Lima, M.V. Donadon, L.S. Leão, Flutter suppression of plates subjected to supersonic flow using passive constrained viscoelastic layers and Golla–Hughes–McTavish method, Aerosp. Sci. Technol. 52 (2016) 70–80, http://dx.doi.org/10.1016/j.ast.2016.02.022.

[35] X.-D. Yang, T.-J. Yu, W. Zhang, Y.J. Qian, M.H. Yao, Damping effect on supersonic panel flutter of composite plate with viscoelastic mid-layer, Compos. Struct. 137 (2016) 105–113, http://dx.doi.org/10.1016/j.compstruct.2015.11.020.

[36] W.-H. Shin, I.-K. Oh, J.-H Han, I. Lee, Aeroelastic characteristics of cylindrical hybrid composite panels with viscoelastic damping treatments, J. Sound Vib. 296 (1) (2006) 99–116, http://dx.doi.org/10.1016/j.jsv.2006.01.068.

[37] W.-H. Shin, I.-K. Oh, I. Lee, Nonlinear flutter of aerothermally buckled composite shells with damping treatments, J. Sound Vib. 324 (3) (2009) 556–569, http://dx.doi.org/10.1016/j.jsv.2009.02.022.

[38] S. Mahmoudkhani, M. Sadeghmanesh, H. Haddadpour, Aero-thermo-elastic stability analysis of sandwich viscoelastic cylindrical shells in supersonic airflow, Compos. Struct. 147 (2016) 185–196, http://dx.doi.org/10.1016/j.compstruct.2016.03.020.

[39] X. Wang, Z. Yang, W. Wang, W. Tian, Nonlinear viscoelastic heated panel flutter with aerodynamic loading exerted on both surfaces, J. Sound Vib. 409 (2017) 306–317, http://dx.doi.org/10.1016/j.jsv.2017.07.033.

[40] L.-q. Ye, Z.-y. Ye, K. Ye, J. Wu, Aeroelastic stability and nonlinear flutter analysis of viscoelastic heated panel in shock-dominated flows, Aerosp. Sci. Technol. 117 (2021) 106909, http://dx.doi.org/10.1016/j.ast.2021.106909.

[41] E. Carrera, E. Zappino, Aeroelastic analysis of pinched panels in supersonic flow changing with altitude, J. Spacecr. Rockets 51 (1) (2014) 187–199, http://dx.doi.org/10.2514/1.A32363.

[42] E. Zappino, E. Carrera, M. Cinefra, Aeroelastic analysis of composite pinched panels using higher-order shell elements, J. Spacecr. Rockets 52 (3) (2015) 999–1003, http://dx.doi.org/10.2514/1.A32986.

[43] V. Birman, L. Librescu, Supersonic flutter of shear deformable laminated composite flat panels, J. Sound Vib. 139 (2) (1990) 265–275, http://dx.doi.org/10.1016/0022-460X(90)90887-6.

[44] M. Botshekanan Dehkordi, S.M.R. Khalili, E. E. Carrera, Non-linear transient dynamic analysis of sandwich plate with composite face-sheets embedded with shape memory alloy wires and flexible core- based on the mixed LW (layer-wise)/ESL (equivalent single layer) models, Composites B 87 (2016) 59–74, https://www.sciencedirect.com/science/article/pii/S1359836815006101.

[45] A. Pagani, S. Valvano, E. Carrera, Analysis of laminated composites and sandwich structures by variable-kinematic MITC9 plate elements, J. Sandw. Struct. Mater. 20 (1) (2018) 4–41, http://dx.doi.org/10.1177/1099636216650988.

[46] J.N. Reddy, Mechanics of Laminated Composite Plates and Shells – Theory and Analysis, second ed., CRC Press, Boca Raton, 2004.

[47] B. Arash, W. Exner, R. Rolfes, Viscoelastic damage behavior of fiber reinforced nanoparticle-filled epoxy nanocomposites: Multiscale modeling and experimental validation, Composites B 174 (2019) 107005, http://dx.doi.org/10.1016/j.compositesb.2019.107005.

[48] B. Arash, W. Exner, R. Rolfes, A viscoelastic damage model for nanoparticle/epoxy nanocomposites at finite strain: A multiscale approach, J. Mech. Phys. Solids 128 (2019) 162–180, http://dx.doi.org/10.1016/j.jmps.2019.04.004.

[49] B. Bahtiri, B. Arash, S. Scheffler, M. Jux, R. Rolfes, A machine learning-based viscoelastic–viscoplastic model for epoxy nanocomposites with moisture content, Comput. Methods Appl. Mech. Engrg. 415 (2023) 116293, http://dx.doi.org/10.1016/j.cma.2023.116293.

[50] W.T.. Koiter, A consistent first approximation in the general theory of thinelastic shells, in: Proceedings of First Symposium on the Theory of Thin Elastic Shells, North-Holland, Amsterdam, 1959, http://resolver.tudelft.nl/uuid:13cb5366-bbdc-4dd1-8514-951302217759.

[51] V. Birman, C.W. Bert, On the choice of shear correction factor in sandwich structures, J. Sandw. Struct. Mater. 4 (2002) 83–95, http://dx.doi.org/10.1177/1099636202004001180.

[52] J.A. Moreira, F. Moleiro, A.L. Araújo, Layerwise electro-elastic user-elements in Abaqus for static and free vibration analysis of piezoelectric composite plates, Mech. Adv. Mater. Struct. 29 (21) (2022) 3109–3121, http://dx.doi.org/10.1080/15376494.2021.1886381.

[53] H. Ashley, G. Zartarian, Piston theory-a new aerodynamic tool for the aeroelastician, J. Aeronaut. Sci. 23 (12) (1956) 1109–1118, http://dx.doi.org/10.2514/8.3740.

[54] Y. Chai, W. Gao, B. Ankay, F.M. Li, C. Zhang, Aeroelastic analysis and flutter control of wings and panels: A review, Int. J. Mech. Syst. Dyn. 1 (1) (2021) 5–34, http://dx.doi.org/10.1002/msd2.12015.

[55] N.J. Pagano, Exact solutions for rectangular bidirectional composites and sandwich plates, J. Compos. Mater. 4 (1970) 20–34, http://dx.doi.org/10.1177/002199837000400102.

[56] E. Carrera, S. Brischetto, Analysis of thickness locking in classical, refined and mixed multilayered plate theories, Compos. Struct. 82 (4) (2008) 549–562, http://dx.doi.org/10.1016/j.compstruct.2007.02.002.

[57] M. Petrolo, E. Carrera, M. Cinefra, E. Zappino, Finite Element Analysis of Structures Through Unified Formulation, John Wiley & Sons, 2014, http://dx.doi.org/10.1002/9781118536643.

[58] R. Unger, B. Arash, W. Exner, R. Rolfes, Effect of temperature on the viscoelastic damage behaviour of nanoparticle/epoxy nanocomposites: Constitutive modelling and experimental validation, Polymer 191 (2020) 122265, http://dx.doi.org/10.1016/j.polymer.2020.122265.